Linear and Nonlinear Rheological Properties of Poly(Propylene Carbonate)

YANG Lixin

Linear and Nonlinear Rheological Properties of Poly(Propylene Carbonate)

ポリ(プロピレンカーボネート)の線型
および非線型粘弾性特性

YANG Lixin

杨 丽欣

CONTENTS

Chapter 1 Introduction

1.1 Background of a CO_2-Based Biodegradable Polymer PPC

Plastics have been extensively used in various fields in our life due to their cheap price and great conveniences. Among plastic materials, common plastics including polyethylene (PE), polypropylene (PP), polystyrene (PS), and poly(vinyl chloride) (PVC) are mostly used.[1] Due to the serious environmental pollution caused by plastics, people intend to decrease the usage of common plastics and are interested in degradable polymers to reduce the white pollution problem. The strong demand for degradable polymers promotes the study and industrial development of such materials. In the past, various degradable polymers have emerged including both natural and synthetic polymers.[2] Natural polymers such as starch and cellulose are rich in resources and cheap, but have poor mechanical properties, which severely limit their application. In contrast to natural polymers, synthetic degradable polymers have relatively good and adjustable mechanical properties, despite that their prices are higher than common plastics.

CO_2-based polycarbonates are copolymers of CO_2 and epoxides, and their synthesis has been first reported by Inoue et al. in the 1970s.[3] CO_2-based polymers are biodegradable by waste landfill and incineration only generating CO_2 and H_2O. Although the consumption of CO_2 in the production of CO_2-based polymers cannot compensate the large amount of CO_2 emission, this use of CO_2 provides a way to make products from low-cost and renewable materials. There are several CO_2-based polycarbonates including poly(ethylene carbonate) (PEC), poly(propylene carbonate) (PPC), and poly(cyclohexane carbonate) (PCHC).[4] Among them, PCHC has good mechanical properties and thermal stability, however, it is not suitable for massive industrial production due to its high price and difficult processability.[4,5] PEC cannot be used as plastics because of its low glass temperature and weak mechanical properties.[4,6] Compared to PCHC and PEC, PPC has lower costs, and relatively good mechanical

properties and thermal stability, and PPC also shows good gas barrier properties, high transparency, and biodegradability, which are of high industrial importance.[4] Figure 1.1 shows the examples of wide applications of PPC products used as disposable products (a, d), barrier and packing materials (b, c, e, g), foam materials (h, f), polymer electrolytes, biomedical materials, etc.[4] In recent years, the production volume of PPC has rapidly increased from 1,000 ton/year in 2008 to more than 20,000 ton/year in 2012, showing a good development prospect.[7,8]

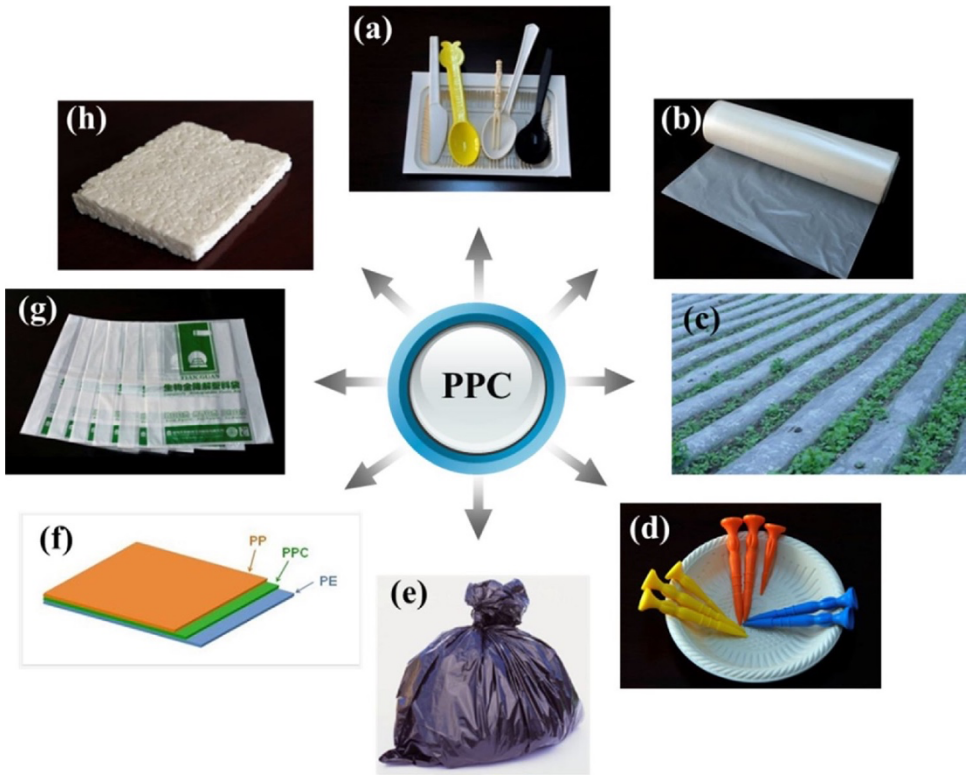

Figure 1.1 Example of applications of PPC in various fields: (a) disposable products, (b) preservation bag, (c) agricultural film, (d) golf tee, (e) garbage bag, (f) laminated barrier composite, (g) shopping bags and (h) foam board. Copied from Ref. 4 with permission.

In the past, mechanical strength, thermal properties, biodegradability, and gas barrier property of PPC have been extensively studied. However, higher price, brittleness, and thermal stability still limit the industrial production and commercial application of PPC.[7-9] For these problems, many researchers focus on the development of various

catalysts and polymerization of PPC to improve catalytic efficiency and control the molecular structure.[10] In addition, physical and chemical modification of PPC have also been widely reported to improve its mechanical and thermal properties.[6,11,12] Physical modification, mainly blending PPC with other degradable polymers/non-degradable polymers/inorganic fillers,[6] is often used because of easy process and excellent effect. Improvements have been obtained from previous studies of PPC modification.[6] However, it is difficult to further optimize the material properties, partly due to the lack of knowledge on the fundamental rheological properties of PPC.

1.2 Rheology of Polymer Melts

Rheology is the study of flow and deformation of materials.[13] Rheology is very useful in many fields and products such as polymer, coating, food, cosmetics, etc. These materials are known to have an internal hierarchical structure and hence exhibit a complex rheological response.

It is well-known that rheological properties are very sensitive to molecular characteristics of polymers such as molecular weight, molecular weight distribution, branching, and cross-linking.[14] Using rheology as an analytical tool, it is possible to relate some characteristic rheological parameters to molecular structures of polymers. Various molecular models have been proposed so far to describe the rheological properties of polymers.[15-18]

Rheology can also help us to predict and optimize the processing of polymer melts, and design molecular structure to obtain desired products. Based on this background, rheology is important in both science and industry of polymers. Two basic aspects of rheology, including linear rheology under small or slow deformations and nonlinear rheology under large and fast deformations, are separately discussed below.

1.2.1 Linear Rheology

Linear viscoelastic (LVE) properties are the simplest and fundamental properties in rheology, where stress and strain have a linear relationship under small strain. Therefore, LVE properties of polymers essentially reflect the dynamics of polymers in vicinity of the equilibrium state. Many studies for various polymers have been extensively studied so far.[19]

Several simple shear experiments such as stress relaxation under a constant strain, creep and recovery under constant stress, and small amplitude oscillatory shear under a dynamic strain, can characterize the linear response of polymers. The obtained linear response functions from several different LVE tests are essentially equivalent to each other, and it is possible to transform the data from one test to any other test by Fourier and Laplace transforms.[20]

Dynamic oscillatory shear measurements are widely used for polymer melts because of easy conduction by applying a sinusoidal small strain $\gamma(t) = \gamma_0 \sin \omega t$ (where γ_0 is the strain amplitude) at various angular frequencies ω using a rotational rheometer. The obtained stress $\sigma(t)$ can be expressed as $\sigma(t) = \sigma_0 \sin(\omega t + \delta)$, where δ is the phase difference between $\sigma(t)$ and $\gamma(t)$. From the oscillatory shear measurements, dynamic modulus $G^*(\omega)$ (= $G'(\omega) + iG''(\omega)$, where $G'(\omega)$ and $G''(\omega)$ are the storage and loss modulus, respectively at ω, and i is the imaginary unit) can be obtained from the following relationship:

$$\sigma(t)/\gamma_0 = G'(\omega) \sin \omega t + G''(\omega) \cos \omega t \quad (1\text{-}1)$$

Here, $G'(\omega)$ and $G''(\omega)$ are equivalent to $(\sigma_0(\omega)/\gamma_0) \cos \delta$ and $(\sigma_0(\omega)/\gamma_0) \sin \delta$, respectively.[19,20]

It is well-known that polymer melts exhibit viscoelastic responses over a wide range of ω, as shown in Figure 1.2 as an example. At the higher ω range than the cross point of G' and G'' ($\approx 1/\tau_e$, where τ_e is the characteristic time at the short time scale), which is called transition region, small segments can move and change the local conformation

of polymers. At the middle ω range between two cross points of G' and G'', G' exhibits a wide plateau, which reflects the entropic rubbery elasticity of polymers and is called the rubber plateau region. At the low ω range ($\leq 1/\tau_d$, where τ_d is the characteristic time at the long-time scale), polymer chains have enough time to move as a whole and then exhibit liquid-like behavior.

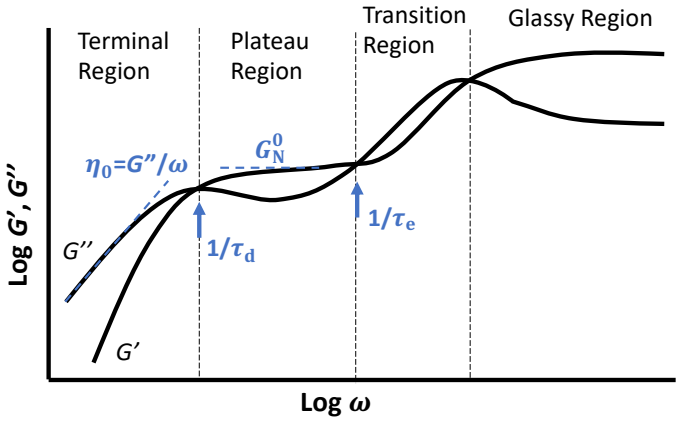

Figure 1.2 Typical linear viscoelastic curves of polymers.

Polymer melts typically exhibit a wide frequency dependence of the modulus, ranging from several to ten orders of magnitude. However, it is difficult to measure such a wide ω range in the experiment. LVE of polymer melts strongly depends on temperature, and shifting the modulus at temperature T in the direction of the frequency is equivalent to the modulus at different temperature T'. This relationship is the so-called empirical time-temperature superposition (tTS) principle.[19] If the reference temperature is set to T_r, the modulus at any arbitrary temperature T can be expressed as follows:

$$G^*(\omega; T_r) = (\rho(T_r)T_r/\rho(T)T)G^*(a_T\omega; T) \qquad (1\text{-}2)$$

Here, $G^*(\omega; T_r)$ and $G^*(a_T\omega; T)$ are the dynamic modulus at temperatures T_r and T, respectively, where the latter is horizontally shifted by the factor a_T in a logarithmic scale. $\rho(T_r)T_r/\rho(T)T$ is the vertical shift factor considering the difference in polymer density $\rho(T)$ and temperature T in Kelvin unit from that at T_r. By applying tTS, master curves of $G^*(\omega)$ under wider ω range can be obtained. According to massive experimental results, empirical tTS is applicable to many polymer melts, and their

temperature dependence of a_T can be uniquely determined irrespective of polymer species by adequately setting T_r.[19]

Some important LVE parameters, which characterize the rheological properties of polymers, can be obtained from the master curves of G' and G'' as shown in Figure 1.2. Plateau modulus G_N^0, zero-shear viscosity η_0, and terminal relaxation time τ_d are typical LVE parameters to determine the rubbery region and terminal relaxation behavior of polymer melts. It has been reported that when the molecular weight of polymers is sufficiently high, the viscoelastic curves of polymers exhibit a wide rubber plateau region. The plateau modulus G_N^0 can be estimated from the plateau region, and it is independent of molecular weight, its distribution nor branching, but depends on polymer species.[21,22] In analogy to the rubbery elasticity, the entanglement molecular weight M_e is defined from G_N^0. In Figure 1.3, after normalizing G' and G'' by related linear rheological parameters, G' and G'' overlapped well for PMMA and PS with same Z ($\approx$ 15).[23]

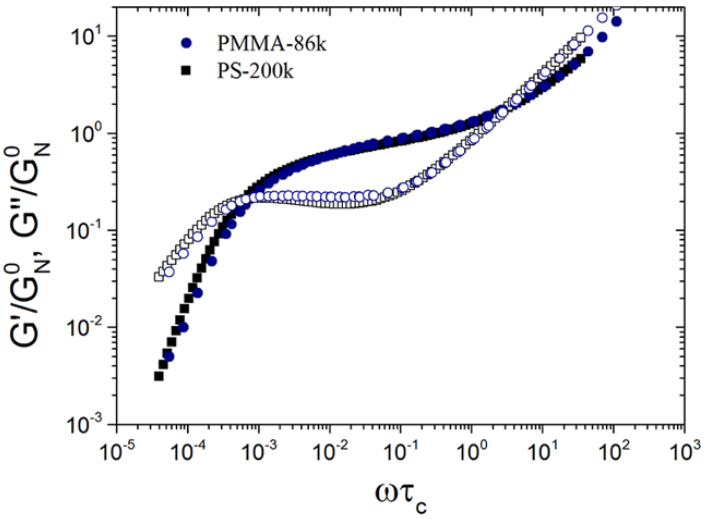

Figure 1.3 Normalized G' and G'' for PMMA and PS. Copied from Ref. 23 with permission.

The zero-shear viscosity η_0 is defined as $\eta_0 = \lim_{\omega \to 0}(G''/\omega)$ at the terminal region. From earlier studies, η_0 has a strong molecular weight M_w dependence as shown in Figure

1.4.[24] For many polymer species, a critical molecular weight M_c exists. When $M_w < M_c$, η_0 increases with M_w as $\eta_0 \propto M_w$. When $M_w > M_c$, η_0 increases with M_w as $\eta_0 \propto M_w^{3.4}$. η_0 and M_c values themselves depend on the polymer species as well as measured temperature, however, the scaling behavior of η_0 against M_w itself is universal for many polymer liquids including melts and dense solutions.[19,24] Besides, the relation $M_c \sim 2M_e$ has been observed for many polymer liquids.

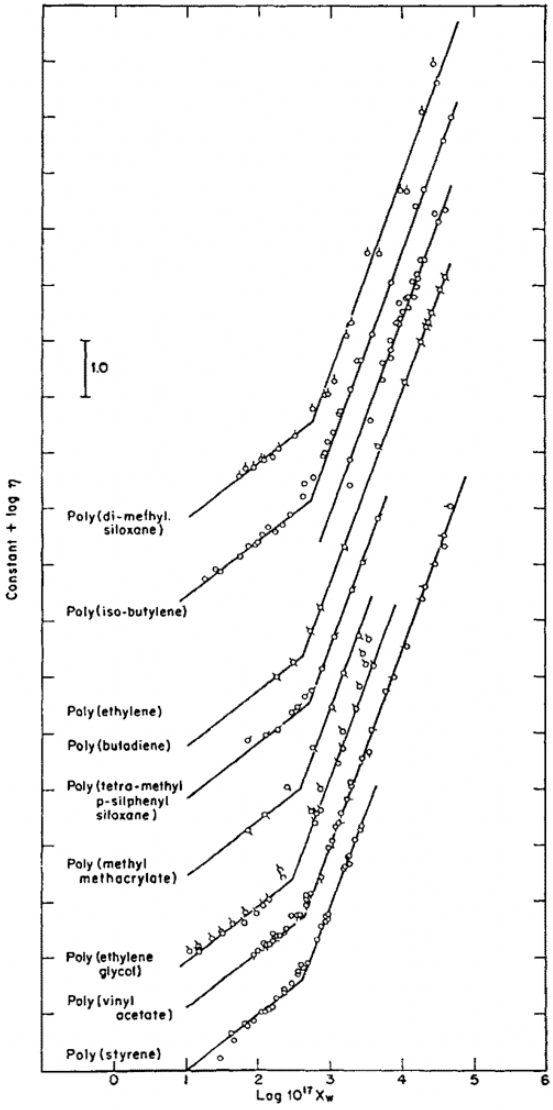

Figure 1.4 Double-logarithmic plot of zero-shear viscosity against molecular weight for various polymer melts. The dataset of each polymer was arbitrarily shifted in both horizontally and vertically for clarity. Copied from Ref. 24 with permission.

With the development of polymer rheology, some fundamental theories have been established to describe and predict the rheological properties of polymers based on the motion of chains. In the Bead-spring model, Rouse[15] regarded a polymer chain as a series of Brownian beads connected by Hookean springs, as schematically shown in Figure 1.5. In this model, the bead diffusivity was denoted by the monomeric friction ζ. This model describes the dynamics of polymers with $M_w < M_c$.

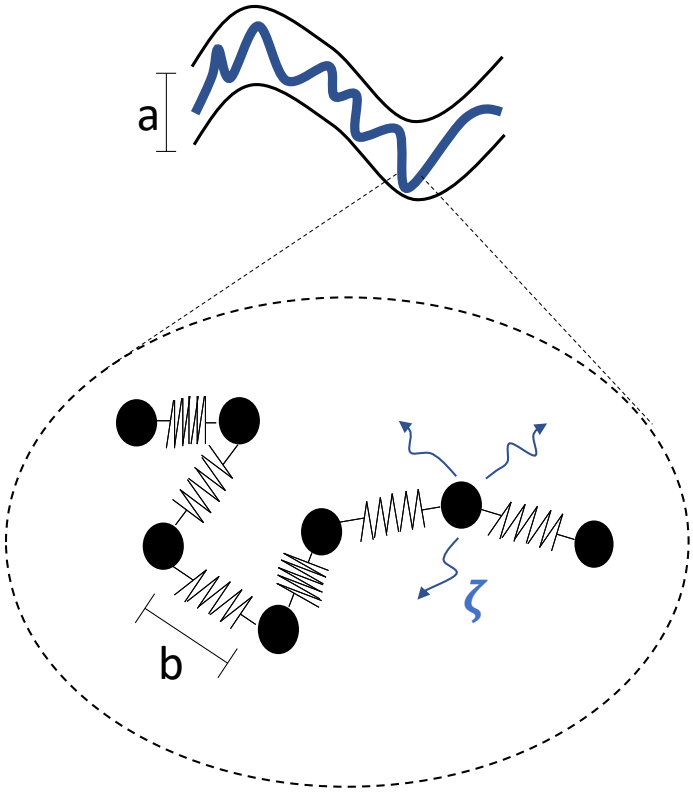

Figure 1.5 Schematic illustration of the tube and Rouse model.

Meanwhile, de Gennes and Doi-Edwards proposed and developed the tube theory to explain the dynamics of polymers with $M_w > M_c$.[17,18] As shown in Figure 1.5, the polymer motion is retarded from the Rouse behavior when $M_w > M_c$. The retarded dynamics is considered to be due to entanglement among polymers, though the molecular origin is still unclear. In the tube theory, the retarded dynamics is described by the motion of a Rouse chain moving in a tube-shaped constraint. This tube is characterized by its diameter, which determines the intensity of the motion constraint and is directly related to M_e. For quantitative prediction of experiments, lots of modified

theories have been proposed. Among them, the theory by Likhtman and McLeish[25] is widely accepted for the prediction of linear viscoelasticity of linear monodispersed polymers.

Figure 1.6 shows the example for polystyrene melts with M_w = 290k, 750k, 2540k at 180 °C. The agreement with the data is attained via the parameters that consist of G_N^0, τ_e and M_e. In addition, a characteristic parameter of the LM model is the constraint-release intensity c_v, which controls the renewal rate of the tube. In the case of Figure 1.6, c_v is chosen at 1.0.

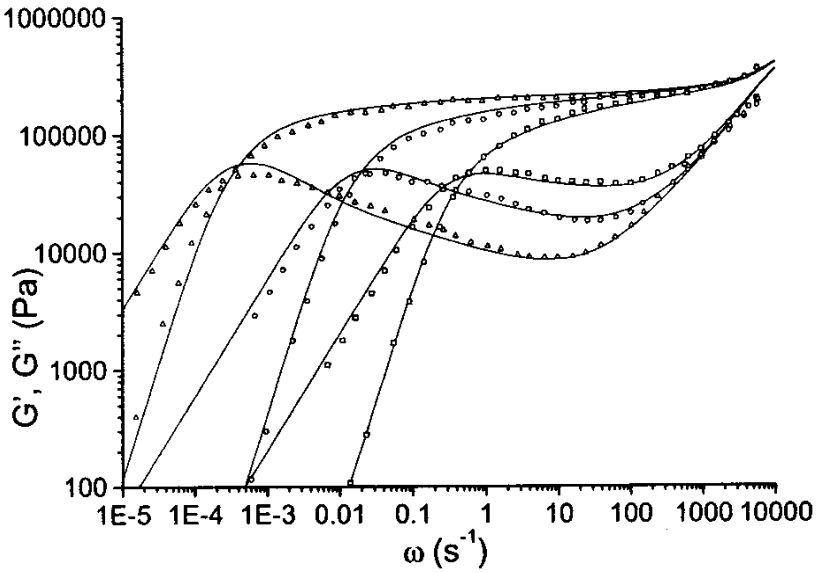

Figure 1.6 LM model prediction of G' and G'' for PS melts. Copied from Ref. 25 with permission.

1.2.2 Nonlinear Rheology

In contrast to LVE, nonlinear viscoelastic (NLVE) properties of polymers under fast and large deformations reflect the polymer dynamics in nonequilibrium state, and they are related to the practical processing. The rheological responses of polymers are known to strongly depend on the deformation manner such as shear, elongation, compression, etc. Understanding and modeling the nonlinear elongational flow

behaviors are still necessary. Two kinds of nonlinear flow properties, that is, under shear and uniaxial elongation, have been widely studied for polymer melts.[19]

Shear rheology

Nonlinear shear rheological properties for polymers are widely investigated using rotational rheometers with a cone-plate geometry to achieve a constant shear rate $\dot{\gamma}$ in a sample, as shown in Figure 1.7. For high-shear, capillary rheometers are also used.

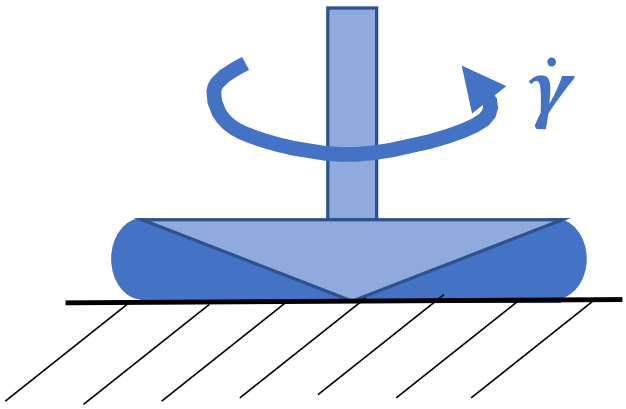

Figure 1.7 Schematic illustration of shear flow measurements using a cone and plate geometry under a constant shear rate $\dot{\gamma}$.

Startup shear flow behavior at different $\dot{\gamma}$ of entangled polymer melts has been widely investigated.[26-28] Figure 1.8 shows typical shear viscosity growth curves of an entangled PS melt with M_w = 182.1 kg/mol at 180 °C.[27] Transient viscosity $\eta^+(t)$ at low $\dot{\gamma}$ follows the linear envelope transformed from the LVE data. At high $\dot{\gamma}$, $\eta^+(t)$ decreases obviously compared with those at low $\dot{\gamma}$, and exhibits overshoot and then reaches a steady value. This stress overshoot behavior has been attributed to the orientation of chains from simulation studies.[29-31]

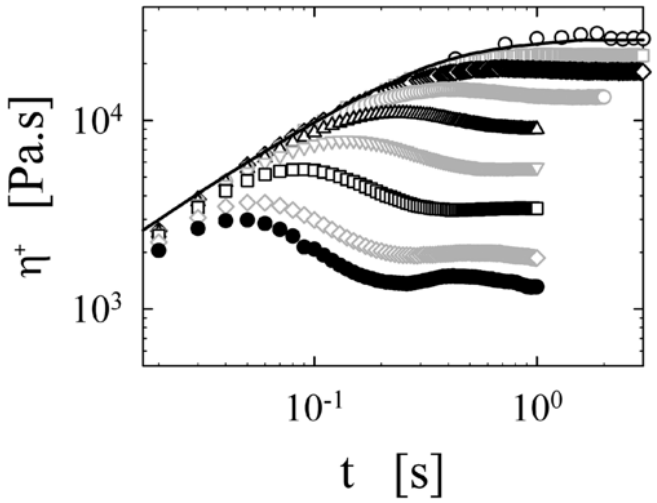

Figure 1.8 Startup shear viscosity of an entangled PS melt at different $\dot{\gamma}$ (from top to bottom: 0.10, 1.78, 3.16, 5.62, 10.0, 17.8, 31.6, 56.2, 70.0 s^{-1}, T = 180 °C). Copied from Ref. 27 with permission.

Figure 1.9 shows the steady-state shear viscosities $\eta(\dot{\gamma})$ normalized by the zero-shear viscosity η_0 as a function of $Wi_D = \dot{\gamma}\tau_d$, for polyisoprene (PI) (circle, M_w = 60 kg/mol at 10 °C) and PS (triangle, M_w = 182.1 kg/mol at 180 °C) reported by Snijkers et al.[27] Solid curve (PI) and broken curve (PS) are linear viscoelastic curves from the dynamic measurements. Steady-state shear viscosities first keep constant up to around $Wi_D \approx 1$, and then decrease at high Wi_d. A relationship between the viscosity and the shear rate, $\eta(\dot{\gamma}) \propto \dot{\gamma}^{-a}$ $(0.2 \leq a \leq 0.9)$, is reported for various polymers.[32] This shear-thinning behavior is induced by the orientation of polymer chains. $\eta^*(\omega)|_{\omega=\dot{\gamma}}$ against ω from dynamic shear (solid and broken curves) and $\eta(\dot{\gamma})$ against $\dot{\gamma}$ from shear flows (symbols) are in good agreement in Figure 1.8. This relationship, $\eta^*(\omega)|_{\omega=\dot{\gamma}} = \eta(\dot{\gamma})$, is known as the empirical Cox-Merz rule,[33] and the validity of this rule is confirmed in many polymers,[19] though the mechanism is unknown.

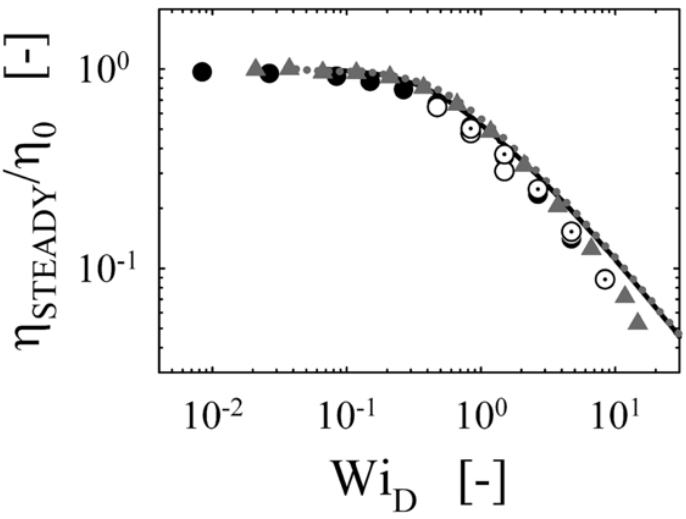

Figure 1.9 Normalized steady-state shear viscosities against Wi_D of PI (circle) and PS (triangle). Copied from Ref. 27 with permission.

Elongational rheology

Nonlinear elongational rheology focuses on the responses of fluids stretched in one or more directions or compressed. Uniaxial elongation is the simplest elongation flow where the velocity gradient $\nabla \boldsymbol{v}$ is defined as:

$$\nabla \boldsymbol{v} = \dot{\varepsilon} \begin{bmatrix} 1 & 0 & 0 \\ 0 & -1/2 & 0 \\ 0 & 0 & -1/2 \end{bmatrix} \quad (1\text{-}3)$$

Here, $\dot{\varepsilon}$ is the elongational rate, indicating stretch along the x direction and equal compression along y and z directions.

The filament stretching rheometer (FSR) has been designed and developed by several researchers to obtain reliable uniaxial elongational data.[34,35] The sample is molded to a cylinder shape and put between two parallel stainless plates. As shown in Figure 1.10, the mid-plane diameter D of the filament is obtained by laser and a photo detector during the stretch, and a constant rate is attained by a feedback loop. The Hencky strain ε is defined as $\varepsilon = 2\ln(D_0/D_t) = \ln(L_t/L_0)$ where D_0 is the initial diameter, D_t is the transient diameter, L_0 is the initial length, and L_t is the transient length.

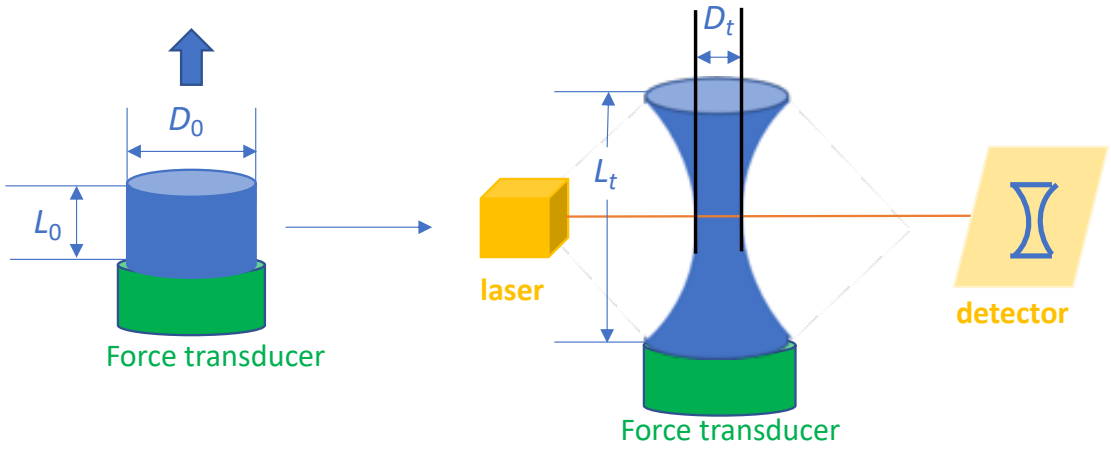

Figure 1.10 Schematic illustration of uniaxial elongational deformation of the sample while measuring the midplane diameter in FSR.

Uniaxial elongational behaviors of well-defined PS melts have been mostly investigated in earlier research.[36-39] Figure 1.11 shows the transient elongational viscosity $\eta_E^+(t)$ of PS with M_w = 200 kg/mol and M_w/M_n = 1.04. At high $\dot{\varepsilon}$, $\eta_E^+(t)$ deviates from the linear envelope to the higher side, which is different from the corresponding shear viscosity data. The elongational transient viscosity finally reaches a steady-state value at large Hencky strain. As $\dot{\varepsilon}$ increased, the deviation of the viscosity becomes more pronounced, while the final steady-state viscosity becomes lower.

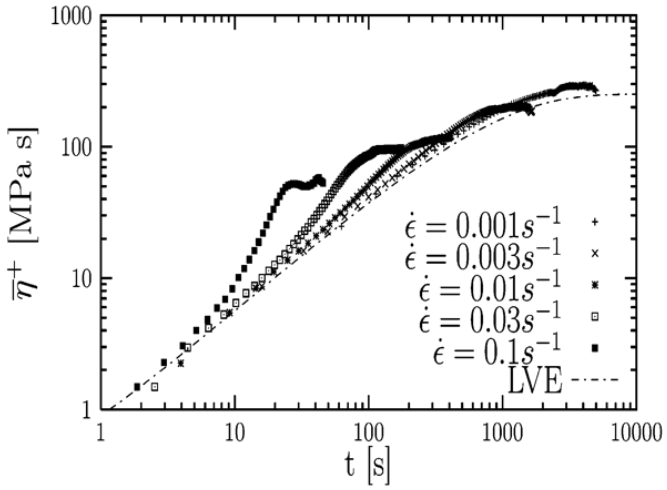

Figure 1.11 Transient elongational viscosity of an entangled PS with M_w = 200k and M_w/M_n = 1.04 at different $\dot{\varepsilon}$ at 130 °C. Copied from Ref. 36 with permission.

Different from the shear viscosity, the elongational viscosity does not converge to a universal curve. Figure 1.12 shows the steady-state elongational viscosity $\eta_E(\dot{\varepsilon})$ normalized by zero shear viscosity η_0 as a function of $\dot{\varepsilon}\tau_d$ for PS, poly(tert-butyl styrene) (PtBS), poly(methyl methacrylate) (PMMA) reported by Morelly et al.[23] and PI, poly(n-butyl acrylate) (PnBA) by Sridhar et al.[40] In Figure 1.12, PS, PI, and PMMA shows similar decreasing elongational viscosity with increasing of $\dot{\varepsilon}$ with a slope of approximately −0.5, but the viscosity of PtBS weakly deviates from that of other polymers. In particular, PnBA shows a clear upturn of η_E at high $\dot{\varepsilon}$.

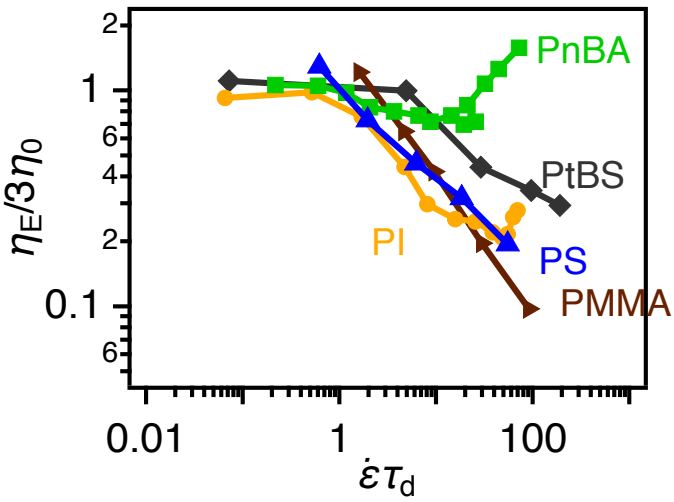

Figure 1.12 Steady-state elongational viscosity $\eta_E(\dot{\varepsilon})$ normalized by $3\eta_0$ as a function of $\dot{\varepsilon}\tau_d$ for several polymer melts, PS (M_w = 290k), PMMA (M_w = 100k), PI (M_w = 145k), PtBS (M_w = 301k), PnBA (M_w = 200k). Reproduced from Ref. 23 and 40 with permission.

Figure 1.13 shows the tube theory prediction with considering the finitely extensible nonlinear elastic (FENE) effect for steady-state elongational viscosities η_E against $\dot{\varepsilon}$.[41] When $\dot{\varepsilon}$ is sufficiently small, η corresponds to the linear volume $3\eta_0$ as seen in region I. When the Weissenberg number Wi_d ($= \dot{\varepsilon}\tau_d$) exceeds unity, that is, $\dot{\varepsilon} > 1/\tau_d$, the tube segments begin to orient along the elongation direction, this orientation induces the reduction of viscosity in region II. At high $\dot{\varepsilon}$, i.e., Rouse Weissenberg number Wi_R (=

$\dot{\varepsilon}\tau_R$, where τ_R is the Rouse relaxation time) exceeds unity, the chain begins to stretch, resulting in the increase of viscosity in region III. Finally, the chain reaches the maximum stretch, and the viscosity reaches a constant value, which is higher than that predicted from LVE (i.e., $3\eta_0$). The maximum stretch ratio of polymer chains, λ_{max}, determines the elongational viscosity in region IV. This prediction fails to predict the elongational viscosity shown in Figure 1.12, that is, PS, PtBS and PMMA do not show any upturn of η_E even at high $\dot{\varepsilon}$. In addition, the theory predicts a decrease in $\eta_E(\dot{\varepsilon})$ against $\dot{\varepsilon}$ with a slope of −1 in region II, but the experimental results in Figure 1.12 show a decrease with ca. −0.5.

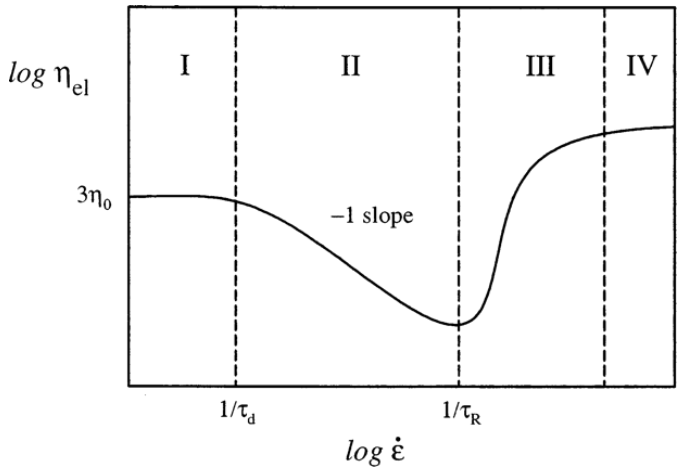

Figure 1.13 Steady-state elongational viscosity as a function of elongation rate predicted from the tube theory. Copied from Ref. 41 with permission.

To resolve the above discrepancy between experiments and theory, several models have been proposed. Narimissa et al.[42] compared reported experimental data with the predictions by their tube model incorporating the extended interchain pressure (EIP) effect. Both transient and steady-state elongational viscosity η_E of PS, PMMA, and PtBS are in quantitative agreement with the model if the tube relaxation time is newly introduced and tuned for the data. However, the physics of this new parameter is not specified.

Another model, that is, the stretch/orientation-induced reduction of friction (SORF) is proposed.[43] In the basic tube theory, the fiction coefficient of polymers is considered to be constant even under fast flow due to local equilibrium assumption. However, when the elongational rate $\dot{\varepsilon}$ is very fast ($>1/\tau_R$), the friction coefficient may change because the polymer chains are highly anisotropic, as shown in Figure 1.14. Ianniruberto et al.[43] confirmed such a change of friction by atomistic molecular simulations.

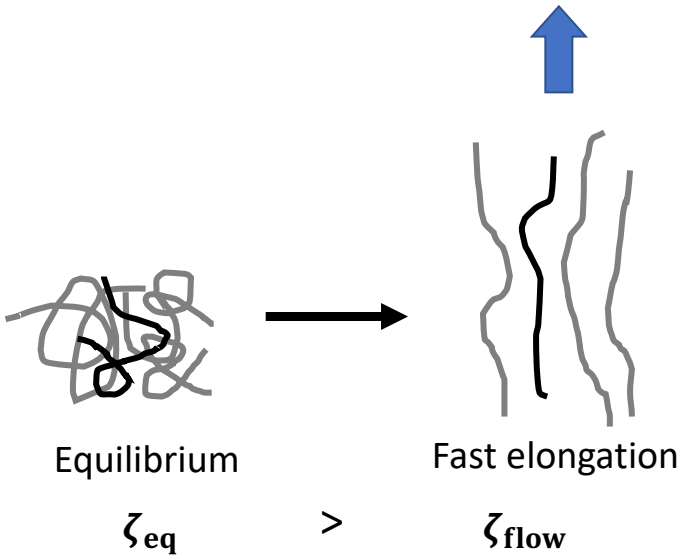

Figure 1.14 Schematic illustration of flow-induced friction reduction in polymer melts under fast elongation.

With this hypothesis, Yaoita et al.[44] examined the elongational data for PS melts by primitive chain network (PCN) simulations including FENE and SORF effects for first time, as shown in Figure 1.15. PCN without FENE simulations (black dotted curves) and PCN-FENE without SORF simulations (black broken curves) overestimate the experimental data at high elongational rates for PS100k, PS200k, and PS390k. Only PCN-FENE with SORF simulations can reasonably predict the decreasing elongational viscosity, indicating that the friction change happens to PS melts under fast elongation.

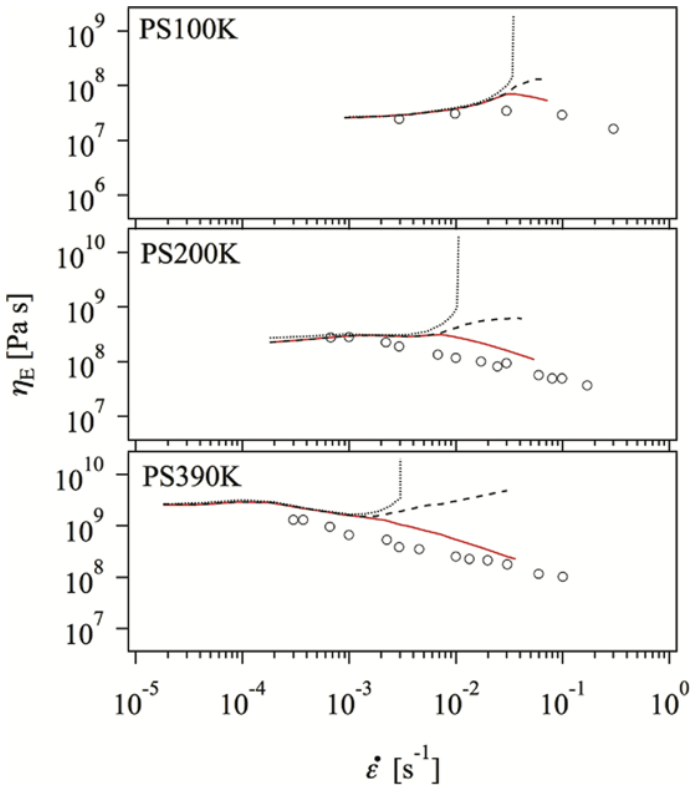

Figure 1.15 Steady-state elongational viscosity against elongational rate at 130 °C for PS melts. Experimental data are shown with unfilled circle. PCN without FENE results are shown with black dotted curves. PCN-FENE results with and without friction reduction are shown with red solid curves and black broken curves. Reproduced from Ref. 44 with permission.

1.3 Rheology of PPC

Although understanding the basic rheological properties is important in polymer melts, systematic rheological studies on PPC, especially using well-defined and characterized samples having different molecular weights with narrow distributions, are very rare.

Regarding LVE properties of PPC, Thorat et al.[45] synthesized a series of aliphatic polycarbonates including PPC with a molecular weight of 28.9 kg/mol and polydispersity of 3.83, and conducted dynamic shear measurements. Ning et al.[46] reported the plateau modulus of PPC as 0.18 MPa according to the crossover modulus of G' and G'' using the data by Thorat et al. Meanwhile, Cao et al.[47] used three commercial PPC samples with the molecular weight of 48~92 kg/mol and M_w/M_n about

2, and estimated the plateau modulus as 0.3~0.7 MPa according to the integration method of G''. Lin et al.[48] obtained the plateau modulus as 0.15 MPa according to G' at minimum $\tan\delta$, and the entanglement molecular weight M_e as 21.3 kg/mol. Unlike other reported synthetic polymers such as PS, commercial PPC products are usually with broad molecular weight distribution and contain non-negligible impurities (low molecular weight compounds, etc), which make it difficult to discuss the rheological data correctly. There are many studies on the dynamic modulus of PPC/polymer blends and composites, but these studies are for the compatibility of PPC and other polymers or fillers.[50-52]

Concerning nonlinear rheology, there are no systematic studies. Li et al.[49] reported the nonlinear shear properties of PPCs having different molecular weights (M_n = 26.9–144.6 kg/mol) with broad distributions (M_w/M_n = 1.92–3.87). They used a melt indexer to discuss the effect of pressure, without discussion on molecular rheology.

1.4 Thesis Outline

Based on the background mentioned in the previous sections, from both scientific and industrial viewpoints, it is necessary to systematically explore the rheological properties of PPC. The aim of this Ph.D. thesis is to investigate both linear and nonlinear rheological properties of PPC with a series of well-prepared samples. The obtained data shall be compared with those for other polymers, and the rheology of PPC will be characterized.

After this introductory chapter, a few chapters are dedicated to the following purposes. In Chapter 2, a series of PPC samples having different molecular weights with relatively narrow distributions were prepared by the precipitation fractionation of a commercial PPC, which leads to solving the problem of sample uncertainties in the previous studies.

In Chapter 3, LVE of the PPC samples was examined, and LVE parameters such as G_N^0 and η_0 were obtained. The data of PPCs in this thesis were compared to the reported data for PPC and other polymers for evaluation. Finally, the dynamic moduli were compared with the Likhtman-McLeish model on the universality of LVE properties of PPC.

In Chapter 4, the nonlinear shear and uniaxial elongation viscoelastic properties of the PPCs are investigated. In the shear measurements, the shear rate dependence of steady-state viscosities of the PPCs was evaluated and confirmed if the empirical Cox-Merz rule is not violated. In the uniaxial elongational measurements, the viscosity growth curves and the steady-state viscosities were systematically obtained. The elongational data of the PPCs are directly compared to those of other polymers.

1.5 References

1. Geyer R, Jambeck J R, Law K L. *Science Advances*, **2017**, 3(7): e1700782.
2. Chandra R, Rustgi R. *Progress in Polymer Science*, **1998**, 23(7): 1273-1335.
3. Inoue S, Koinuma H, Tsuruta T. *Journal of Polymer Science Part B: Polymer Letters*, **1969**, 7(4): 287-292.
4. Xu Y, Lin L, Xiao M, et al. *Progress in Polymer Science*, **2018**, 80: 163-182.
5. Koning C, Wildeson J, Parton R, et al. *Polymer*, **2001**, 42(9): 3995-4004.
6. Muthuraj R, Mekonnen T. *Polymer*, **2018**, 145: 348-373.
7. Rieger B, Künkel A, Coates G, et al, "*Synthetic biodegradable polymers*", (2012), Springer Science & Business Media, P29-P48.
8. Qin Y, Wang X. *Biotechnology Journal*, **2010**, 5(11): 1164-1180.
9. Luinstra G A. *Polymer Reviews*, **2008**, 48(1): 192-219.
10. Klaus S, Lehenmeier M W, Anderson C E, et al. *Coordination Chemistry Reviews*, **2011**, 255(13-14): 1460-1479.
11. Feng J Y, Gao L J, Chen B, et al. *Chemistry letters*, **2013**, 42(7): 714-716.

12. Yao M, Mai F, Deng H, et al. *Journal of Applied Polymer Science*, **2011**, 120(6): 3565-3573.
13. Barnes H A, Hutton J F, Walters K, "*An Introduction to Rheology*", (**1989**), Elsevier.
14. Gahleitner M. *Progress in Polymer Science*, **2001**, 26(6): 895-944.
15. Rouse Jr P E. *The Journal of Chemical Physics*, **1953**, 21(7): 1272-1280.
16. Zimm B H. *The journal of chemical physics*, **1956**, 24(2): 269-278.
17. de Gennes P G. "*Scaling concepts in polymer physics*", (**1979**), Cornell university press, Ithaca and London.
18. Doi M, Edwards SF, "*The Theory of Polymer Dynamics*", (**1986**), Oxford, Clarendon.
19. Ferry JD, "*Viscoelastic Properties of Polymers*", 3rd ed, (**1980**), John Wiley & Sons Inc, New York.
20. Graessley WW. "*Polymeric Liquids & Networks: Dynamics and Rheology*", (**2008**), Garland Science, London and New York.
21. Masubuchi Y, Doi Y, Uneyama T. *Nihon Reoroji Gakkaishi*, **2020**, 48(4): 177-183.
22. Liu C, He J, Van Ruymbeke E, et al. *Polymer*, **2006**, 47(13): 4461-4479.
23. Morelly S L et al. *Macromolecules*, **2019**, 52(3): 915-922
24. Berry G C, Fox T G. "*The viscosity of polymers and their concentrated solutions*", (**1968**), Springer, Berlin, Heidelberg, P261-P357.
25. Likhtman A E, McLeish T C B. *Macromolecules*, **2002**, 35(16): 6332-6343.
26. Auhl D, Ramirez J, Likhtman A E, et al. *Journal of Rheology*, **2008**, 52(3): 801-835.
27. Snijkers F, Vlassopoulos D. *Journal of Rheology*, **2011**, 55(6): 1167-1186.
28. Costanzo S, Huang Q, Ianniruberto G, et al. *Macromolecules*, **2016**, 49(10): 3925-3935.
29. Xie S J, Schweizer K S. *Macromolecules*, **2018**, 51(11): 4185-4200.
30. Cao J, Likhtman A E. *ACS Macro Letters*, **2015**, 4(12): 1376-1381.
31. Becerra D, Córdoba A, Schieber J D. *Macromolecules*, **2021**, 54(17): 8033-8042.

32. Graessley W W. "*The Entanglement Concept in Polymer Rheology*", (**1974**), Springer, Berlin, Heidelberg.
33. Cox W P, Merz E H. *Journal of Polymer Science*, **1958**, 28(118): 619-622.
34. Marin J M R, Huusom J K, Alvarez N J, et al. *Journal of Non-Newtonian Fluid Mechanics*, **2013**, 194: 14-22.
35. McKinley G H, Sridhar T. *Annual Review of Fluid Mechanics*, **2002**, 34(1): 375-415.
36. Bach A, Almdal K, Rasmussen H K, et al. *Macromolecules*, **2003**, 36(14): 5174-5179.
37. Münstedt H. *Journal of Rheology*, **1980**, 24(6): 847-867.
38. Wagner M H, Kheirandish S, Hassager O. *Journal of Rheology*, **2005**, 49(6): 1317-1327.
39. Matsumiya Y, Watanabe H, Masubuchi Y, et al. *Macromolecules*, **2018**, 51(23): 9710-9729.
40. Sridhar T, Acharya M, Nguyen D A, et al. *Macromolecules*, **2014**, 47(1): 379-386.
41. Marrucci G, Ianniruberto G. *Macromolecules*, **2004**, 37(10): 3934-3942.
42. Narimissa E, Poh L, Wagner M H. *Rheologica Acta*, **2021**, 60(4): 163-174.
43. Ianniruberto G, Brasiello A, Marrucci G. *Macromolecules*, **2012**, 45(19): 8058-8066.
44. Yaoita T, Isaki T, Masubuchi Y, et al. *Macromolecules*, **2012**, 45(6): 2773-2782.
45. Thorat S D, Phillips P J, Semenov V, et al. *Journal of Applied Polymer Science*, **2004**, 93(2): 534-544.
46. Ning W, Zhu W, Zhang B, et al. *Chinese Journal of Polymer Science*, **2012**, 30(3): 343-349.
47. Cao C, Yuan L, Feng L, et al. *Polymer Materials Science & Engineering* (Chinese), **2012**, 28(7), 18-21.
48. Lin S, Yu W, Wang X, et al. *Industrial & Engineering Chemistry Research*, **2014**, 53(48): 18411-18419.
49. Li X H, Meng Y Z, Chen G Q, et al. *Journal of Applied Polymer Science*, **2004**, 94(2): 711-716.

50. Ren G, Miao Y, Qiao L, et al. *RSC Advances*, **2015**, 5(62): 49979-49986.

51. Hao Y, Ge H, Han L, et al. *Polymer Bulletin*, **2013**, 70(7): 1991-2003.

52. Li Z, Li W, Zhang H, et al. *Iranian Polymer Journal*, **2015**, 24(10): 861-870.

Chapter 2 Sample Preparation and Characterization

2.1 Sample Preparation

A commercial PPC sample was purchased from Sigma-Aldrich. The company reports that the sample has a number-averaged molecular weight M_n ~ 50 kg/mol by gel permeation chromatography (GPC) with PS standards.

The commercial PPC was treated by precipitation fractionation[1] to prepare the PPC samples having different molecular weights with relatively narrow distribution. The detailed procedure is described as follows, and the schematic illustration is shown in Figure 2.1. PPC (10 g) was dissolved in dichloromethane (CH_2Cl_2) (1 L) at room temperature and the solution was stirred for several hours. Methanol (MeOH) was dropped into the solution until the solution became turbid under stirring, where MeOH was finally added about 750 mL. The solution was first heated up to 45 °C to re-dissolve PPC precipitate and became transparent, and then was cooled down to 35 °C until the precipitate appeared. The solution was kept at 35 °C overnight in a pear-shape bottle to collect the precipitate. After removing the upper supernatant, the first fraction was obtained. This procedure was repeated several times for the remaining upper solution each time until there was no precipitate. PPC fractions were immersed in MeOH and stirred overnight to remove the low molecular weight residues from polymers. After drying the samples under a vacuum oven at 50 °C for several days, the remaining solvent in the samples was completely removed. Finally, six PPC samples with different fractions were prepared and used in the thesis.

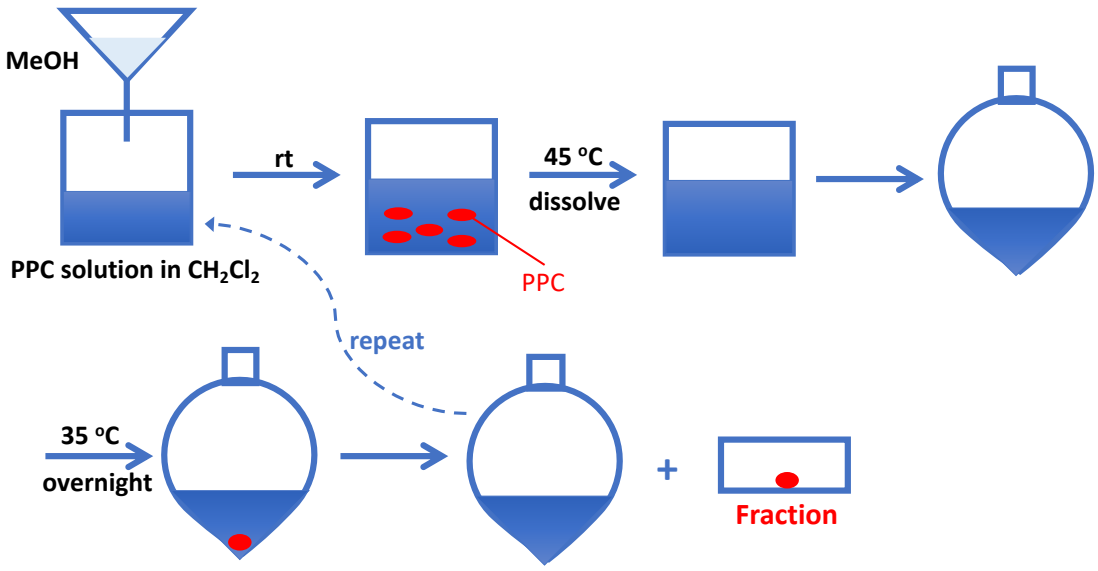

Figure 2.1 Schematic illustration of precipitation fractionation process of PPC.

For the reference of rheological measurements of PPC, a PS sample (M_w = 520 kg/mol, PDI = 1.3) was purchased from Polymer Source, and used as received.

2.2 Sample Characterization

Nuclear Magnetic Resonance (NMR)

Proton nuclear magnetic resonance (^{1}H-NMR) was measured for PPCs to mainly confirm the presence of byproduct propylene carbonate (PC), and also the content of carbonate unit (CU) in PPC. The measurements were performed using Bruker 500MHz NMR spectrometer. The spectrum for the commercial unpurified and fractionated PPCs in $CDCl_3$ is shown in Figure 2.2 (upper and lower panels, respectively). In an ideal PPC, the peaks appear as follows: δ1.34 (t, 3H), δ4.08-4.32 (b, 2H), δ5.00 (s, 1H). It can be seen that the commercial PPC contains a non-negligible amount of low molecular weight PC, but after precipitation PC has been almost completely removed. CU was estimated to be higher than 95%, demonstrating PPC mainly consisted of CU with only a small amount of poly(propylene oxide) (PPO) unit.[2]

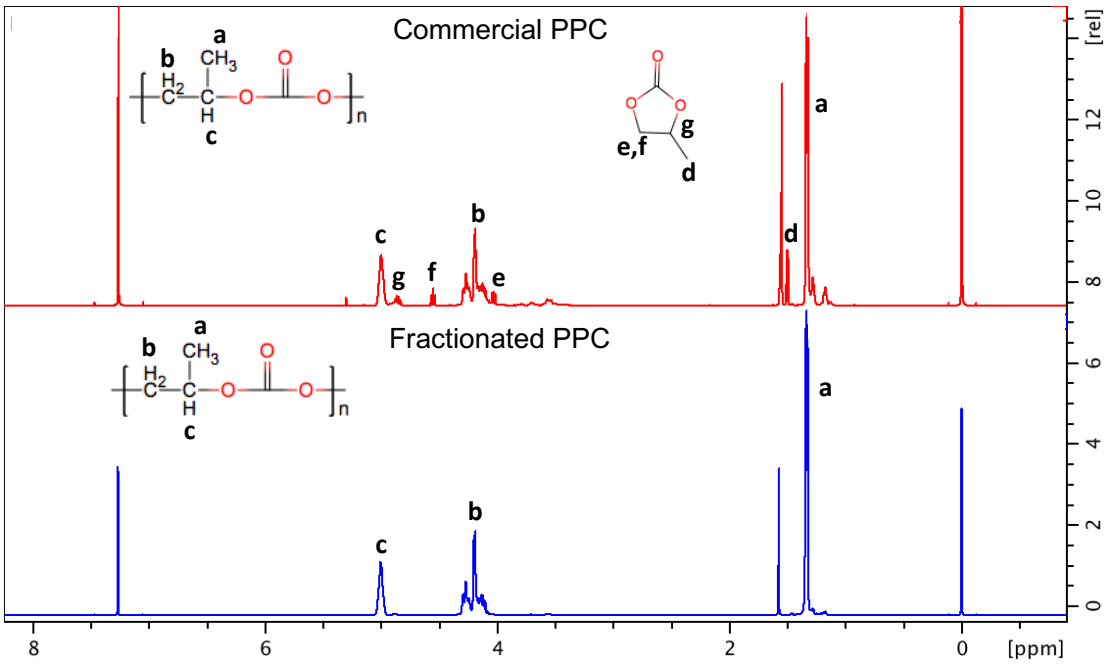

Figure 2.2 ^{1}H-NMR spectrum of commercial and fractionated PPC samples (lower and upper panels, respectively).

Gel Permeation Chromatography (GPC)

Gel permeation chromatography measurements (GPC) were conducted using standard GPC systems (Shimadzu Co.) with a TSK GMH_{XL} column (Tosoh Co.) at 35 °C with polystyrene standards (in the molecular weight range of $5.98 \times 10^5 \sim 1.15 \times 10^3$ g/mol) and an eluent of CH_2Cl_2. The flow rate of the eluent was 1 mL/min, and the sample concentration was ca. 3 mg/mL. The GPC profiles of commercial and fractionated PPC samples detected in a differential refractive index (RI) detector are shown in Figure 2.3. It can be seen that the width of peaks of fractionated PPC samples is clearly narrower than the commercial one. Relative number- and weight-averaged molecular weights (M_n and M_w, respectively) and molecular weight distribution M_w/M_n of the commercial PPC and the fractionated PPC samples are summarized in Table 2.1.

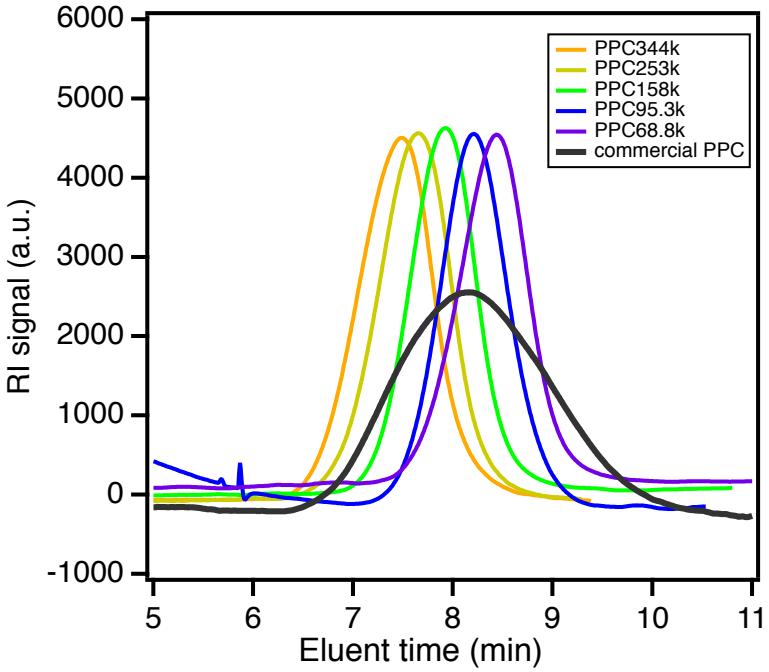

Figure 2.3 GPC profiles of commercial and fractionated PPC samples.

In addition, Figure 2.4 shows a direct comparison of PS520k and a PPC sample, PPC158k, with a similar entanglement number Z (explained later in Chapters 3 and 5) and similar M_w/M_n value (=1.30).

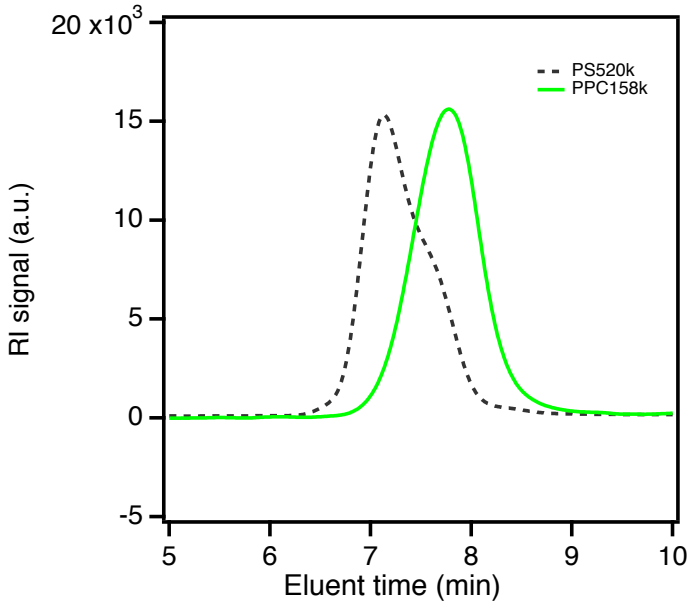

Figure 2.4 GPC profiles of PS520k and PPC158k.

Refractive Index Increment (*dn/dc*)

Refractive index increment, *dn/dc*, was obtained with a RI detector Optilab T-rEX (Wyatt Technology). The wavelength of the incident light was 658 nm and the measurement temperature was set to be 35 °C. A fractionated PPC sample was used. Five solutions of the PPC dissolved in tetrahydrofuran (THF) in the concentration range of 1~10 mg/mL were prepared, and used for measurements. The *dn/dc* value of PPC/THF was estimated from Figure 2.5 as 0.047 ± 0.003 mL/g.

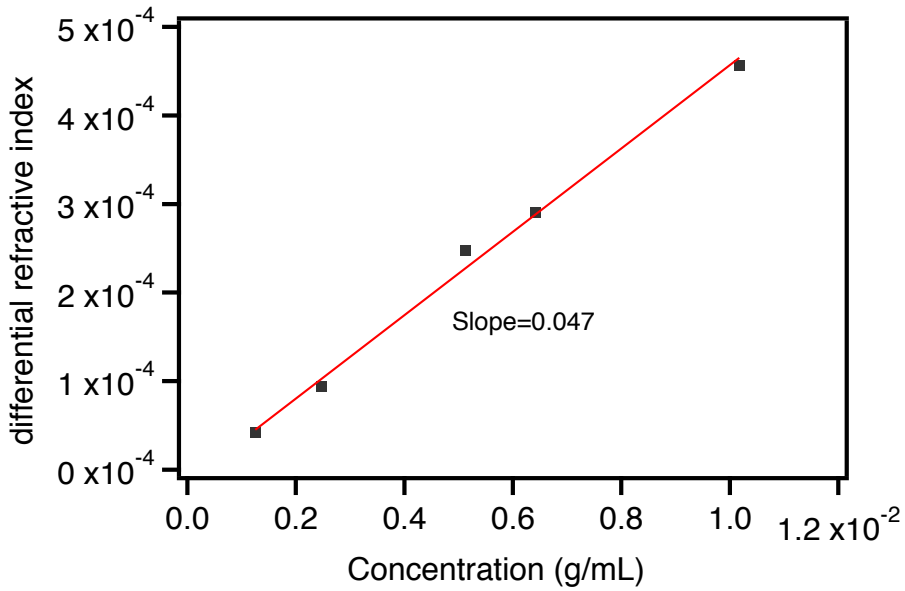

Figure 2.5 Differential refractive index against concentration for a fractionated PPC.

Multi-Angle Light Scattering detection (MALS)

GPC measurements with multi-angle light scattering detection (GPC-MALS) were performed to determine the absolute weight-averaged molecular weight M_w of the samples. GPC-MALS system was mainly equipped with a standard GPC system (Shimadzu Co.) combined with three TSKgel G4000H_{HR} columns (Tosoh Co.) at 40 °C, RI detector (Optilab T-rEX, Wyatt Technology), and MALS detector (DAWN HELEOS-II, Waytt Technology; laser wavelength of 658 nm). THF was used as an eluent. The flow rate was 1 mL/min and the injection volume was 100 μL at each time. Figure 2.6 shows the obtained GPC profiles with M_w traces for fractionated PPC samples. The obtained absolute M_w values are summarized in Table 2.1. The sample

code of the fractionated PPC samples is denoted based on the M_w values obtained from GPC-MALS.

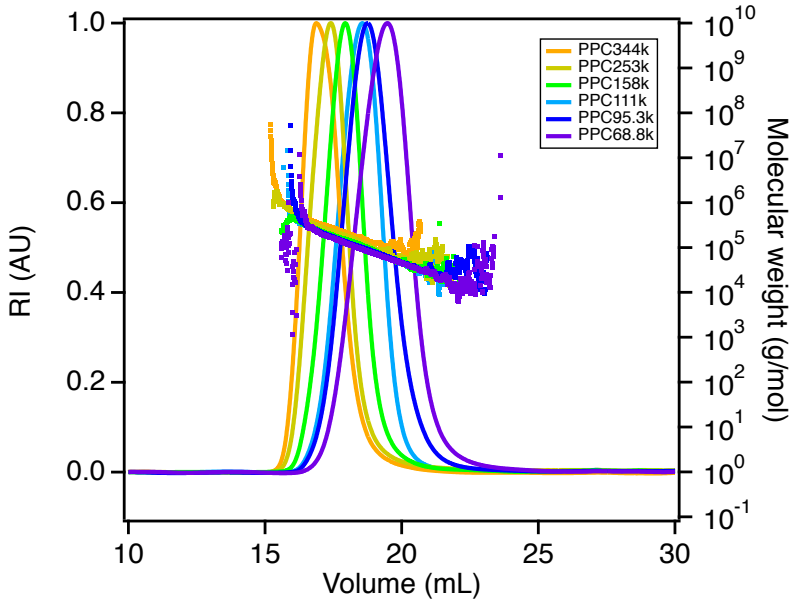

Figure 2.6 GPC profiles of fractionated PPC samples with molecular weight traces.

The sample code, relative molecular weight from GPC with PS standards, absolute molecular weight from MALS, and glass temperature are summarized in Table 2.1.

Table 2.1 Molecular characteristics of PPC samples.

Sample	$M_{n\text{-GPC}}$	$M_{w\text{-GPC}}$	$M_w/M_{n\text{-GPC}}$	$M_{w\text{-MALS}}$	T_g
	kg/mol	kg/mol	-	kg/mol	°C
Commercial PPC	53.2	184	3.46	-	21
PPC344k	320	460	1.44	344	42
PPC253k	256	361	1.41	253	41
PPC158k	181	236	1.30	158	40
PPC111k	107	157	1.30	111	40
PPC95.3k	104	144	1.39	95.3	39
PPC68.8k	73.4	105	1.43	68.8	36

Differential Scanning Calorimetry (DSC)

Differential scanning calorimetry (DSC) measurements were conducted on a Q20 instrument (TA Instruments) under a N_2 atmosphere. PPC samples were first heated from −20 °C to 100 °C at the heating rate of 10 °C/min, and cooled down at the same rate, followed by the second heating process. Figure 2.7 shows the DSC curves of the commercial and fractionated PPC samples. The glass transition temperature T_g is estimated using the midpoint value of transition in DSC curves. The obtained T_g values are listed in Table 2.1.

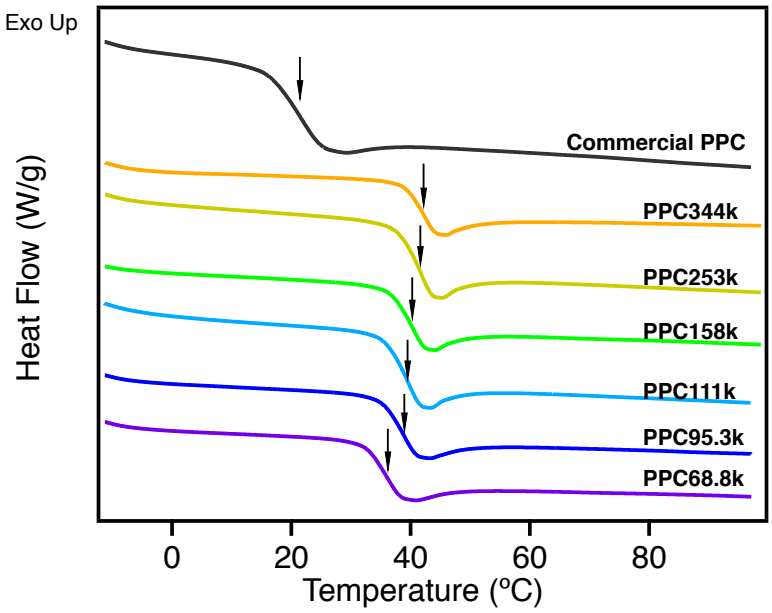

Figure 2.7 DSC curves of commercial and fractionated PPC samples. The arrow indicates the position of T_g for each sample.

Figure 2.8 shows the molecular weight dependence of T_g for PPC. Here, M_n from GPC measurements was used. All fractionated PPC samples have considerably higher T_g values than commercial PPC, where the latter contains a non-negligible amount of low molecular weight compounds such as propylene carbonate (PC) and oligomers, as confirmed from ^{1}H-NMR and GPC results.

The T_g values of the fractionated PPCs slightly decrease with decreasing M_n. The molecular weight dependence of T_g is known to follow the empirical equation proposed by Fox and Flory:[3]

$$T_g = T_{g,\infty} - K_g/M_{n-GPC} \qquad (2\text{-}1)$$

where $T_{g,\infty}$ is T_g at infinite large molecular weight, and K_g is a constant value depending on polymer species. From Figure 2.8 the data for fractionated PPCs can be well-fitted by the equation 2-1 with $T_{g,\infty}$ = 44 °C and K_g = 5.2 × 10^5 K g/mol. T_g of the commercial PPC deviates clearly from the fitting line, indicating that the low molecular weight compounds in the commercial PPC strongly decrease T_g as discussed above.

In Figure 2.8, T_g data for the fractionated PPCs and those reported by Li et al.[4] are compared. Although T_g values by Li et al. are higher than our data, their T_g values in a wide molecular weight range follow the equation with the same K_g and higher $T_{g,\infty}$ value (ca. 5 °C). Note that Li et al. did not describe how they determined the M_n values of their PPC samples.

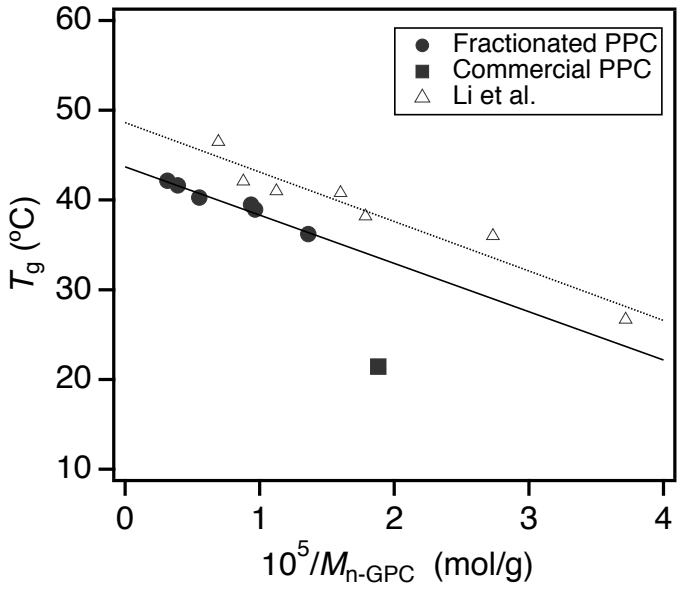

Figure 2.8 T_g plotted against the inverse of $M_{n\text{-}GPC}$ for the commercial and fractionated PPC samples in this thesis, compared with T_g by Li et al.[4]

2.3 References

1. Young R J, Lovell P A. "*Introduction to polymers*", 3rd ed, (**2011**), CRC press, Taylor & Francis Group.
2. Lai M F, Li J, Liu J J. *Journal of Thermal Analysis and Calorimetry*, **2005**, 82(2): 293-298.
3. Fox Jr T G, Flory P J. *Journal of Applied Physics*, **1950**, 21(6): 581-591.
4. Li X H, Meng Y Z, Chen G Q, et al. *Journal of Applied Polymer Science*, **2004**, 94(2): 711-716.

Chapter 3 Linear Viscoelasticity of PPC

3.1 Introduction

Previous linear rheological studies on PPC mainly used commercial products. Commercial PPC contains a large amount of low molecular weight compounds, which could have a great influence on the rheological properties. (In fact, it was already confirmed in the glass transition temperature in Chapter 2.) In addition, the previous studies determined the LVE parameters such as plateau modulus G_N^0 according to different methods. Thorat et al.[1] synthesized a PPC sample (M_w = 28.9 k, M_w/M_n = 3.83) and measured the dynamic modulus of PPC. According to the data by Thorat et al., Ning et al.[2] determined the plateau modulus for PPC as 0.18 MPa from the crossover modulus of G' and G''. Cao et al.[3] estimated the plateau modulus as 0.3-0.7 MPa according to the integration of G'' using three commercial PPC samples (M_w = 48-92 k, M_w/M_n = 2). Lin et al.[4] calculated the plateau modulus for commercial PPC sample (M_w ≈ 235 k) as 0.15 MPa according to G' at the minimum of $\tan\delta$ (= G''/G'). The results of the plateau modulus for PPC in the above previous studies are not consistent with each other and scattered in a wide range (0.15-0.7 MPa). However, in principle, the plateau modulus should be independent of molecular weight and temperature.[5] The main reason for the discrepancy of G_N^0 may be due to the impurities of commercial PPC samples. In addition, it is difficult to directly compare the LVE data for PPC from previous studies because of the insufficient range of frequency. To eliminate the influence of the sample, it is necessary to prepare purified PPC samples and carefully measure the LVE of PPC.

The purpose in Chapter 3 is to investigate the LVE of fractionated PPC samples and obtain LVE parameters such as G_N^0 and zero-shear viscosity η_0. Six PPC samples having different molecular weights with relatively narrow molecular weight distribution were used, as prepared and characterized in Chapter 2. Dynamic oscillatory shear measurements under small strains were conducted for the PPCs at various

temperatures, and master curves of G' and G'' over a wide range of angular frequency ω were obtained according to the time-temperature superposition (tTS) principle. We estimated G_N^0 of the PPCs by different methods, and compared the obtained values to those in earlier studies.[2-4] The molecular weight dependence of η_0 of the PPCs was estimated, and the normalized data were compared with some other polymers. Finally, the spectra of G' and G'' of the PPCs were compared with the Likhtman-McLeish (LM) model.

3.2 Experiments

3.2.1 Samples

Six fractionated PPC samples (i.e., PPC344k, PPC253k, PPC158k, PPC111k, PPC95.3k, and PPC68.8k) used in this Chapter 3 were prepared, and their characteristics were summarized in Chapter 2.

3.2.2 Measurements

A rotational shear rheometer (MCR301, Anton-Paar) was used for small amplitude oscillatory shear (SAOS) measurements equipped with a parallel plate geometry with a diameter of 8 mm. A PPC sample was loaded between two plates at 120 °C. The plates gradually pressed the sample to accommodate the gap, and the final gap value was set to 1 mm. A range of ω of 0.1−100 rad/s was adopted and the stain amplitude was set to 1%, which ensures the linearity of stress. The measurements of the PPC samples were conducted at various temperatures from 60 °C to 140 °C. It was confirmed by GPC that the PPC samples did not thermally degrade during the measurements in this temperature range.

3.3 Results and Discussion

3.3.1 Master Curves of PPC

Figure 3.1 shows the master curves of G', G'' and $\tan\delta$ against ω of the fractionated six PPC samples after performing both a_T and b_T. It can be seen that the master curves

according to the time-temperature superposition (tTS) are obtained in a wide ω range including the Rouse relaxation, entanglement plateau, and terminal regimes. The reference temperature T_r is set as T_g + 60 °C to compensate for the T_g differences of PPC samples (as confirmed in Chapter 2). At high ω ($\geq 10^3$ s^{-1}), both dynamic modulus and tanδ of six PPC samples overlap well because in this region the contribution of large-scale global motion of the chains does not appear. At terminal regime dynamic modulus shifts to lower ω region with increasing of the molecular weight of PPC. This behavior has already been reported for many other polymers.[6,7]

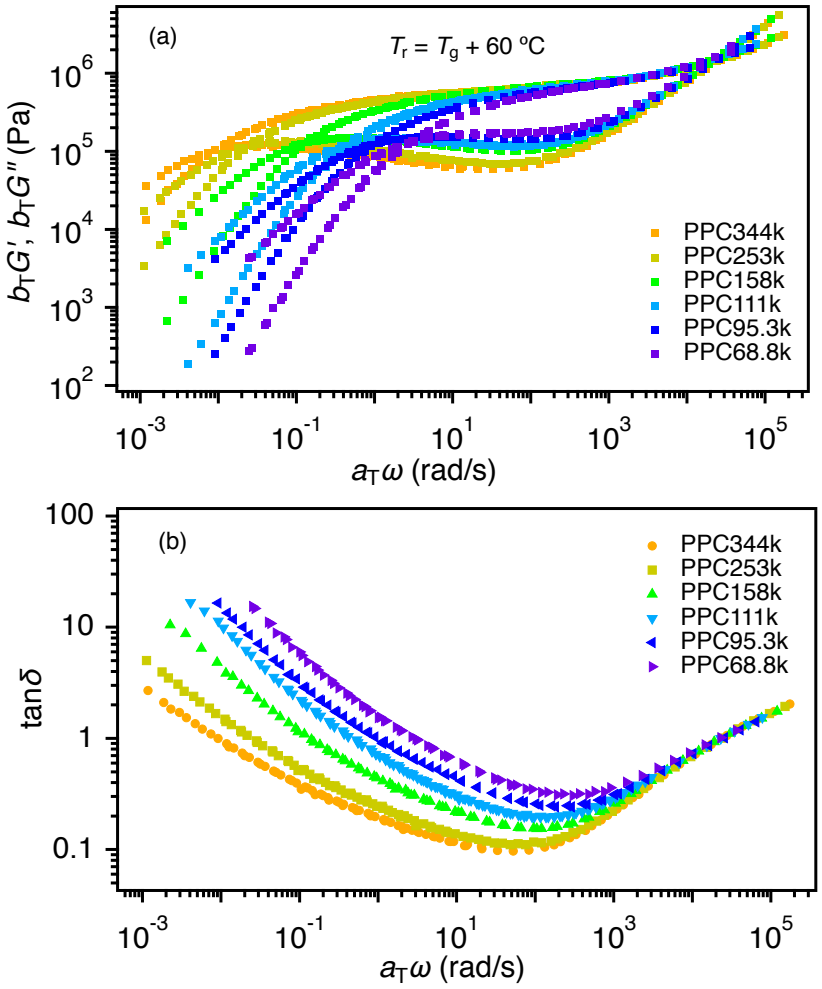

Figure 3.1 (a) Master curves of G' and G'' and (b) tanδ for six fractionated PPC samples reduced at $T_r = T_g + 60$ °C.

After setting T_r, the shift factors a_T and b_T depend only on the polymer species. Figure 3.2 plots the horizontal shift factor a_T and vertical shift factor b_T against the reduced temperature $T - T_r$. From Figure 3.2a, all the a_T values for six PPCs collapse on a curve expressed by the Williams-Landel-Ferry (WLF) equation:[7]

$$\log a_T = \frac{-C_1(T-T_r)}{C_2+(T-T_r)} \qquad (3\text{-}1)$$

Here the parameter values are $C_1 = 6.59$, $C_2 = 121.9$ K and $T_r = T_g + 60$ °C.

The a_T values for reported PPC by Lin et al.[4] are also plotted in Figure 3.2a for comparison to exhibit a good agreement with the data. Note that Lin et al. reported the data at $T_r = 100$ °C, and their data were converted to $T_r = T_g + 60$ °C ($T_g = 28.7$ °C reported in Ref. 4).

Figure 3.2b shows the temperature dependence of the vertical shift factor b_T. In principle, b_T can be written as $\rho(T)T/\rho(T_r)T_r$ where $\rho(T)$ and $\rho(T_r)$ are the melt density of the sample at T and T_r, respectively, taking into account the temperature change and also the resulting density change of the sample. In general, b_T decreases with increasing temperature because of the larger change of melt density than those in temperature. In this study, the density change of PPC according to temperature could not be estimated due to experimental difficulties, and hence b_T was arbitrarily determined to attain the best overlapping of the master curves of G' and G''. In contrast to a_T, the temperature dependence of b_T is much weaker. In Figure 3.2b, b_T scatters among the PPC samples, which is relatively bigger than reported data. This error may be due to a small variation of the sample loading.

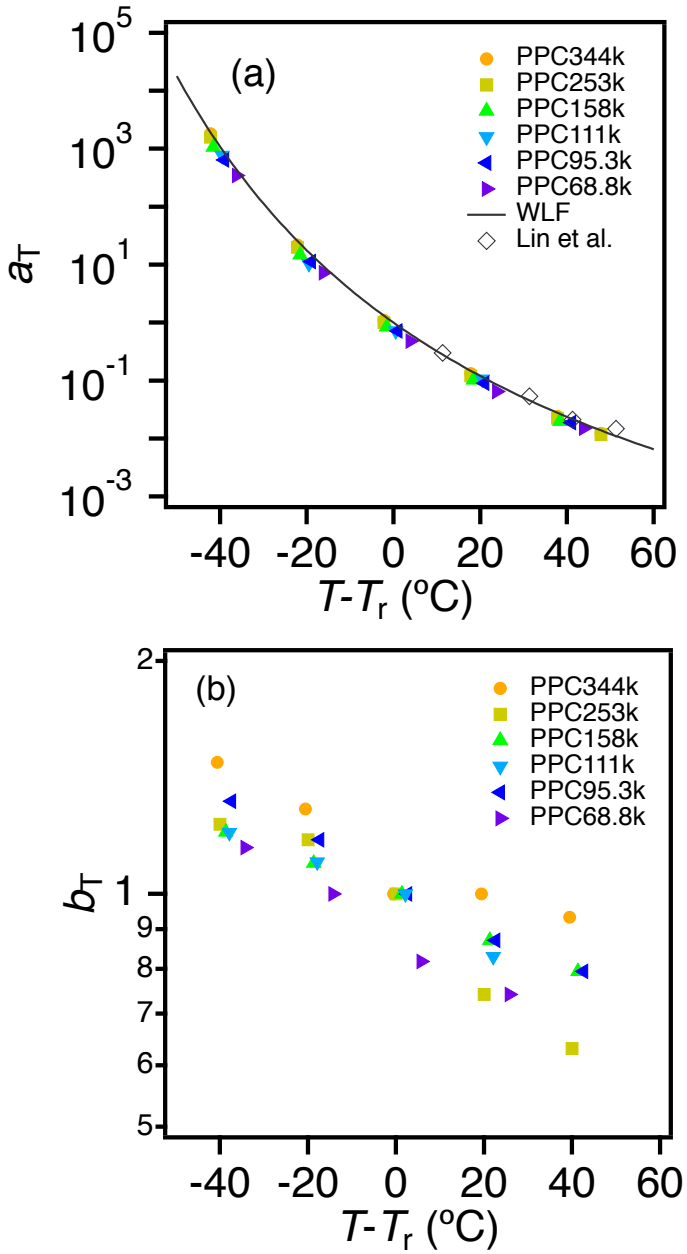

Figure 3.2 Horizontal and vertical shift factors, a_T and b_T, against T - T_r for six PPC samples reduced at $T_r = T_g + 60$ °C.

From Figures 3.1 and 3.2, the empirical tTS principle is confirmed for the PPCs at the reduced reference temperature $T_r = T_g + 60$ °C, based on the dynamic modulus. The temperature dependence of a_T follows the WLF relation. However, a_T slightly deviates among the PPC samples at low temperature, which is probably due to a small error of the fitting to the WLF equation.

To further examine the tTS for the PPCs, vGP-plot is made, which were proposed by van Gurp and Palmen,[8] using the absolute value of complex modulus $|G^*(\omega)|$ and phase difference δ. Trinkle et al.[9] also reported vGP-plot to characterize polydispersity of polymers such as PS, PE, PP, etc. Figure 3.3 shows the plot of δ against $|G^*|$ for the six PPC samples. It can be seen that the master curves of $|G^*|$ basically overlap, indicating that tTS holds for the PPCs. According to Trinkle et al.[9], polymers with similar molecular weight but different molecular weight distribution had similar shape of G^* but the shape was stretched to lower $|G^*|$. Because PPC samples have similar MWD (1.3-1.4), the curves fall to a single curve when G^* is low. When δ is close to 0, $|G^*|$ for all PPC samples show a similar minimum value $|G^*|_{\delta\to\min}$, which is close to the plateau modulus G_N^0.

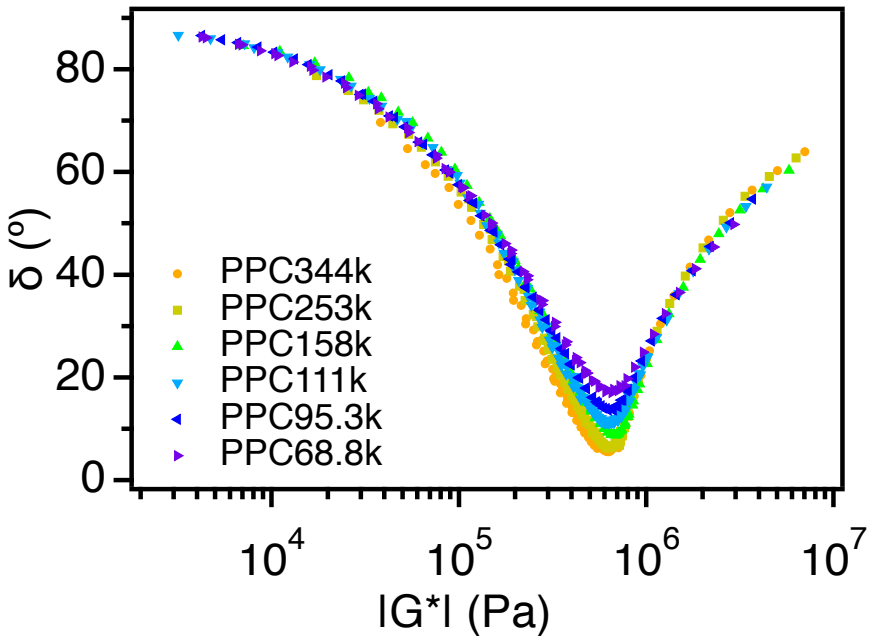

Figure 3.3 The vGP-plot of six PPC samples reduced at $T_r = T_g + 60$ °C.

Figure 3.4 shows the direct comparison of master curves of G' and G'' of PPC253k and reported PPC sample by Lin et al.[4] with a similar molecular weight of 235k. The master curves were compared directly at the same reference temperature $T_r = 100$ °C. As can be seen, the dynamic modulus of PPC253k is approximately 3 times higher than that of Lin et al. in the plateau regime. Considering that the PPC by Lin et al. is a commercial

product, it may contain a large amount of low molecular weight compounds, and hence lead to lower modulus as well as lower T_g (*cf.* Figure 2.8 in Chapter 2). In addition, the molecular weight of PPC by Lin et al. was measured by GPC, which shows a larger value than the data from MALS (as confirmed in Chapter 2). By the limit of incomplete master curve by Lin et al., further discussion is difficult.

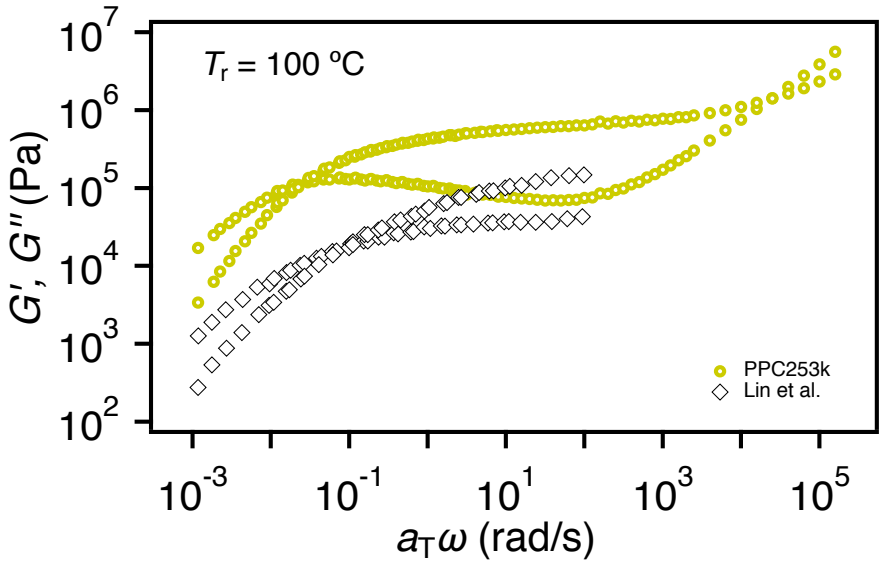

Figure 3.4 Comparison of master curves of G' and G'' of PPC253k with those reported by Lin et al. at T_r = 100 °C.

3.3.2 Plateau Modulus of PPC

From the master curves of G' and G'' in Figure 3.1a, the plateau modulus G_N^0 for the fractionated PPC samples can be estimated according to two reported methods.[5] One is from the integration of G'' in the terminal region as:

$$G^0_{N,Int} = \frac{2}{\pi}\int_{-\infty}^{+\infty} G''(\omega)\, d\ln\omega \qquad (3\text{-}2)$$

Here, the contribution of the Rouse relaxation ($G'' = A\omega^{0.67}$) was subtracted in G'', which was estimated from the extrapolation of overall G'' at high ω.

The other one is estimated from the G' value where tan δ is at minimum:

$$G^0_{N,\tan\delta\to\min} = G'(\omega)|_{tan\delta=min} \qquad (3\text{-}3)$$

The G_N^0 values from these two methods are summarized in Table 3.1. They coincide with each other within an error of 10%. The small change of the G_N^0 values with M_w is mainly due to the experimental error. If the polymer samples are in the well-entangled state, their G_N^0 values should be independent of their molecular weights. The average plateau modulus of the fractionated PPCs was calculated as 670 kPa from $G_{N,Int}^0$ of six PPCs, and this value is used as the plateau modulus of PPC for further discussion.

Using G_N^0, the entanglement molecular weight M_e of PPC can be calculated from the plateau network theory, where Ferry[7] applied this concept to entangled polymers, as follows:

$$M_e = \rho RT/G_N^0 \qquad (3\text{-}4)$$

where ρ is the melt density, for which ρ = 1.26 g/cm^3 was used at room temperature reported by Lin et al.[4] Because of the difficulty of measuring the melt density of PPC at different temperatures (as explained above), here ρ value reported at room temperature was employed.[10] R is the gas constant and T is temperature (373 K in this study). The resultant M_e value is calculated to be 5.9 kg/mol. Our M_e value is considerably lower than that reported by Lin et al. (21.2 kg/mol) because of the different G_N^0 values in Figure 3.5a. Lin et al. considered a prefactor 4/5 based on Doi-Edwards tube model theory[11] to estimate M_e, however, their value is still much higher than 5.9 kg/mol. According to the M_e value of PPC, the related entanglement number $Z = M_w/M_e$ was calculated and summarized in Table 3.1. The molecular weight of the monomer unit for PPC is 102 g/mol. The number of monomers in one entanglement unit is 5900/102 ≈ 58.

Figure 3.5a plots the G_N^0 values against the molecular weight for PPC samples in this thesis and those from previous studies by Cao et al.[3] and Lin et al.[4] The G_N^0 values by Cao et al. are based on the integration method of G'', and show a strong molecular weight dependence. That is, the G_N^0 value from the lowest M_w (=48.2 kg/mol) by Cao et al. is much smaller than the data in this study, however, the G_N^0 values for higher

M_w (=71.2 and 91.9 kg/mol) are similar to G_N^0 in this study. The M_w-dependence of G_N^0 for low M_w might be similar to the earlier studies,[12] and the high M_w samples are highly entangled, exhibiting the saturated G_N^0 value. In contrast, the G_N^0 values in this study are considerably higher than that reported by Lin et al. as G_N^0 = 150 kPa using the G' value at the minimum of tan δ. The reason for the discrepancy can be seen from the direct comparison of G' and G'' in Figure 3.4, in which the dynamic modulus reported by Lin et al. is much lower than our data.

Considering the fact that commercial PPC products were used in most of the previous studies, small molecular weight compounds in the samples might affect G_N^0. According to the Rubinstein-Colby theory,[13] the plateau modulus of well-entangled polymers depends on the polymer volume fraction Φ with a power-law manner written as $G_N^0 \sim \Phi^{2.3}$. It means that 5% low molecular weight compounds in the sample result in 10% decreasing of the plateau modulus. Although the details of the samples by Cao et al.[3] were not reported in their paper, from the similar G_N^0 values we suppose that their samples did not include a large amount of oligomers and low molecular weight compounds. Meanwhile, the sample by Lin et al.[4] may contain massive low molecular weight compounds judging from their lower G_N^0 and T_g values.

Figure 3.5b compares the normalized plateau modulus of the PPCs in this thesis with that of other reported polymers, that is, polybutadiene (PBD), polyisoprene (PI), and PS. By this comparison, it can be examined whether the variation of $G_{N,Int}^0$ values for the fractionated PPCs are within an experimental error or not. The reported data for PBD, PI, and PS are normalized by the averaged $G_{N,Int}^0$ value among the samples with different molecular weights,[5] that is, 1.16 MPa for PBD, 0.38 MPa for PI, and 0.195 MPa for PS. As can be seen in Figure 3.5b, the normalized G_N^0 values for the PPCs are within the scattering of the data for the other polymers.

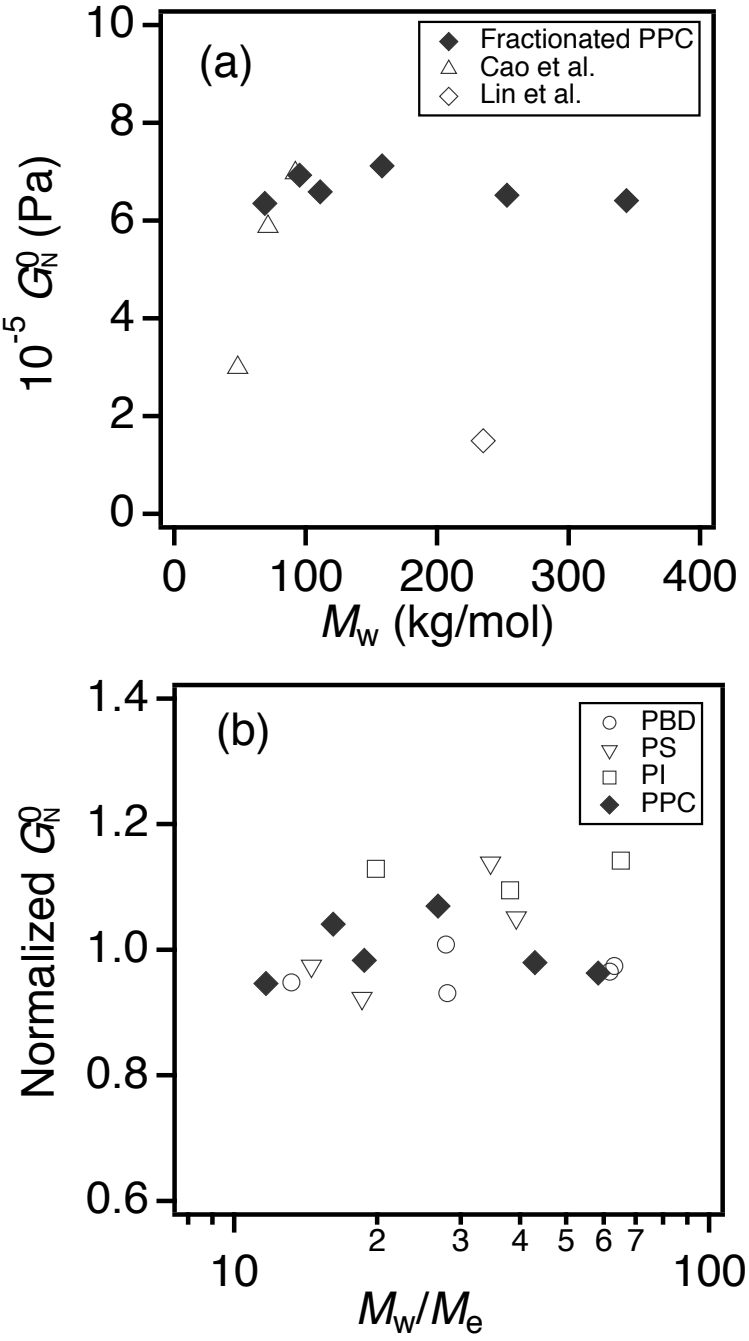

Figure 3.5 (a) The plateau modulus of the fractionated PPCs and PPC reported by Cao et al.[3] and Lin et al.[4] (b) Comparison of the normalized plateau modulus of PPC with reported other polymers, extracted from Ref 5.

Table 3.1 Linear rheological parameters of PPC samples.

Sample	$10^{-5}\ G^0_{N,Int}$ [a] (Pa)	$10^{-5}\ G^0_{N,\tan\delta\to min}$ [b] (Pa)	Z_{MALS} [c]	$10^{-5}\ \eta_0$ [d] (Pa s)
PPC344k	6.4	6.2	58	300
PPC253k	6.5	6.2	43	140
PPC158k	7.1	6.7	27	32
PPC111k	6.6	6.2	19	7.6
PPC95.3k	6.9	6.2	16	4.5
PPC68.8k	6.3	6.0	12	1.6

[a]Estimated from eq. 3-2 at T_g + 60 °C. [b]Estimated from eq. 3-3 at T_g + 60 °C. [c]Calculated from $Z = M_{w\text{-MALS}}/M_e$. [d]Estimated from eq. 3-5 at T_g + 60 °C.

3.3.4 Zero-Shear Viscosity of PPC

The zero-shear viscosity η_0 for the fractionated PPC samples is determined in the terminal region of the LVE spectrum in Figure 3.1 from the following relationship:

$$\eta_0 = \lim_{\omega\to 0}(G''/\omega) \quad (3\text{-}5)$$

The η_0 values obtained are summarized in Table 3.1. Figure 3.6a shows the zero-shear viscosity η_0 against M_w for the PPCs in this study, compared with that reported by Lin et al.[4] η_0 increases with increasing M_w, which can be fitted by $\eta_0 \propto M_w^{3.4\pm0.2}$. This η_0-M_w relationship coincides with previous researches for many other entangled polymer melts.[7] From Figure 3.6a, it is obvious that the zero-shear viscosities of the PPCs in this study are considerably higher than those by Lin et al. at the same molecular weight. This discrepancy can be directly related to the lower modulus as shown in Figure 3.4. Nevertheless, Lin et al. reported a similar power-law relationship as $\eta_0 \propto M_w^{3.5}$ for their PPCs. According to previous experimental results for various polymer melts, it is known that η_0 shows a critical value η_c at critical molecular weight M_c, where the η_0-M_w relationship changes at this critical point. M_c is often related to M_e as $M_c \sim 2M_e$. Here, $M_c = 2M_e = 11.8$ kg/mol for PPC, and η_c is calculated as 410 Pa s from the $\eta_0 \propto M_w^{3.4\pm0.2}$ relationship in Figure 3.6a.

Figure 3.6b shows the normalized molecular weight dependence of η_0 of PPCs in this study compared with that of some reported polymers including PBD, PI, and PS.[14-17] Here, both η_0 and M_w are normalized by η_c and M_e, respectively, for each polymer species to conduct the direct comparison. As can be seen, PPC data are well-overlapped with other reported polymers within a reasonable experimental error.

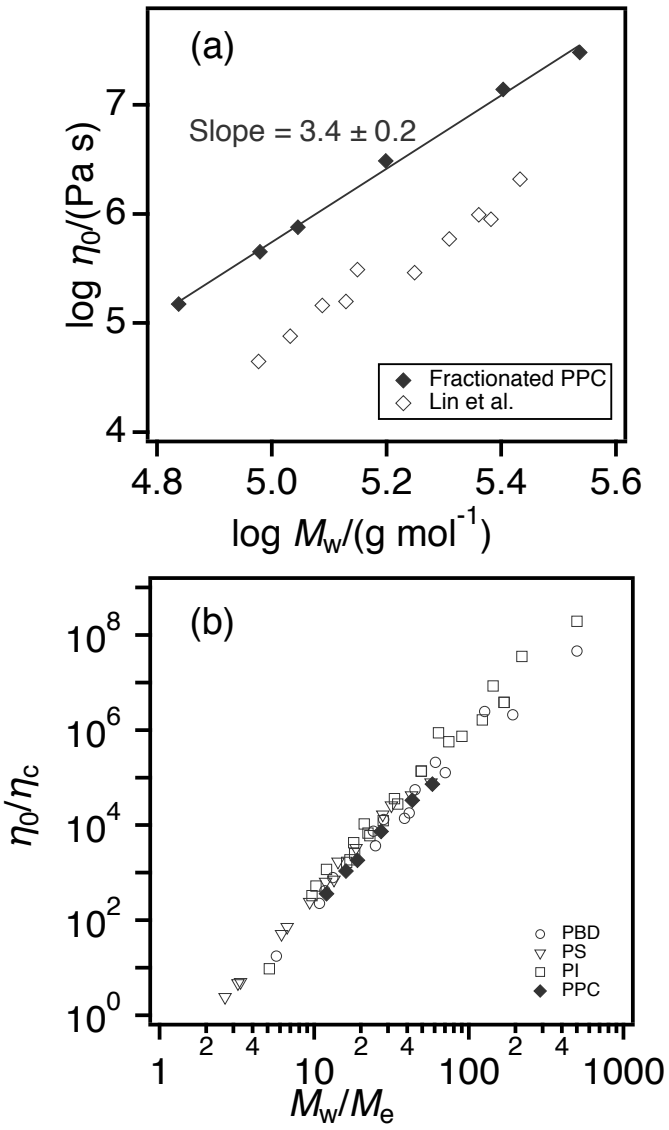

Figure 3.6 (a) Molecular weight M_w dependence of zero-shear viscosity η_0 of six fractionated PPCs in this study and PPCs reported by Lin et al.[4] (b) Normalized zero-shear viscosity of PPCs compared to those reported for other polymers.[14-17]

3.3.5 LM Model Prediction

The molecular weight dependence of the plateau modulus G_N^0 and the zero-shear viscosity η_0 were discussed in the above sub-sections, and they basically follow the established relationship, which is consistent with other polymers. This experimental fact means that LVE properties of PPC can be described by the theory, in which the effect of chemistry is embedded in the parameters: G_N^0, τ_e and Z.

The experimental master curves of G' and G'' for the PPCs in this study are compared with the Likhtman-McLeish (LM) model prediction.[18] The LM model based on the tube theory[11] can be successfully used to quantitatively predict the linear dynamic modulus for linear entangled polymers such as PS, PBD, and PI.[16,17] To fit the data, this model requires three parameters: the entanglement number Z, the entanglement modulus G_e and related relaxation time τ_e. Note that G_e is similar to but different from G_N^0. In addition, as mentioned in Chapter 1, this theory has the other parameter, the so-called constraint-release intensity c_v. These parameters were determined independently. G_e and τ_e were chosen as 900 kPa and 2.0×10^{-4} s, respectively. c_v was set as 1, and the effect of c_v on the dynamic LVE spectra was also examined. Only one remaining parameter, Z_{LM} were varied according to the molecular weight of the samples.

Figure 3.7 shows the G' and G'' divided by G_e against normalized ω by τ_e. The value of the characteristic molecular weight was determined as $M_{e\text{-}LM} = \rho RT/G_e = 4.3$ kg/mol. The related Z_{LM} can be calculated from $Z_{LM} = M_w/M_{e\text{-}LM}$, which are 80, 59, 37, 26, 22, and 16 for the fractionated PPC samples in the order from higher to lower M_w. Note here that G_e and $M_{e\text{-}LM}$ were considered as model dependent parameters, which is not the same with the experimentally estimated G_N^0. In fact, G_e = 900 kPa is 34% higher than G_N^0 = 670 kPa for the PPCs in this study.

Finally, c_v is considered to change the entire relaxation spectrum. Due to the slightly broad molecular weight distribution of the current PPC samples, PPC data slightly show

slower and broader terminal relaxation. This effect of the molecular weight dependence is not considered in the theory and is not compensated by the tuning of c_v.

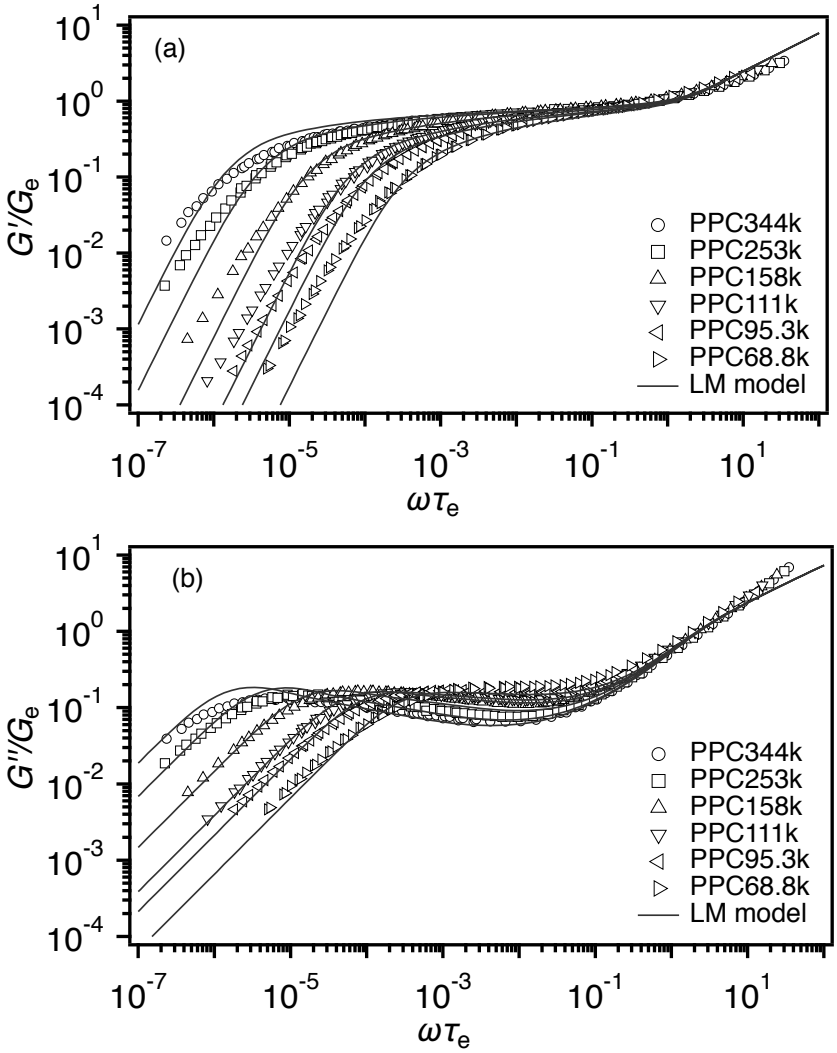

Figure 3.7 Comparison of (a) G'/G_e and (b) G''/G_e against $\omega\tau_e$ between the experimental PPC data (symbols) and LM model predictions (curves) using $Z_{LM} = M_{w\text{-MALS}}/M_{e\text{-LM}}$.

3.4 Conclusion

We investigated the linear viscoelasticity of the fractionated six PPC samples with different molecular weights and relatively narrow molecular weight distributions. The plateau modulus G_N^0 of PPC was estimated as 670 kPa, and M_e as 5.9 kg/mol. The zero-shear viscosity η_0 and molecular weight of PPC follow the relationship of $\eta_0 \propto M_w^{3.4\pm0.2}$.

The LVE parameters of our PPC samples are consistent with empirical laws according to the other reported polymers such as PS. G_N^0 data are different from earlier studies on PPC which may be due to the large amount of low molecular weight compounds in PPC in earlier studies. In addition, the master curves of G' and G'' for the fractionated PPCs are in good agreement with the LM model prediction. But broader terminal relaxation due to non-negligible molecular weight distribution was confirmed.

3.5 References

1. Thorat S D, Phillips P J, Semenov V, et al. *Journal of Applied Polymer Science*, **2004**, 93(2): 534-544.
2. Ning W, Zhu W, Zhang B, et al. *Chinese Journal of Polymer Science*, **2012**, 30(3): 343-349.
3. Cao C, Yuan L, Feng L, Wang J, Gu X, *Polymer Materials Science & Engineering* (Chinese), **2012**, 28(7), 18-21.
4. Lin S, Yu W, Wang X, et al. *Industrial & Engineering Chemistry Research*, **2014**, 53(48): 18411-18419.
5. Liu C, He J, Van Ruymbeke E, et al. *Polymer*, **2006**, 47(13): 4461-4479.
6. Onogi S, Masuda T, Kitagawa K. *Macromolecules*, **1970**, 3(2): 109-116.
7. Ferry JD, "*Viscoelastic properties of polymers*", 3rd ed, (**1980**), John Wiley & Sons Inc, New York.
8. Van Gurp M, Palmen J. *Rheology Bulletin*, **1998**, 67(1): 5-8.
9. Trinkle S, Friedrich C. *Rheologica Acta*, **2001**, 40(4): 322-328.
10. Brandrup J, Immergut EH, Grulke EA, "*Polymer Handbook*", 4th ed, (**1999**), Wiley, New York.
11. Doi M, Edwards SF, "*The Theory of Polymer Dynamics*", (**1986**), Clarendon, Oxford.
12. Masubuchi Y, Doi Y, Uneyama T. *Nihon Reoroji Gakkaishi*, **2020**, 48(4): 177-183.
13. Colby R H, Rubinstein M. *Macromolecules*, **1990**, 23(10): 2753-2757.
14. De Rosa M E, Winter H H. *Rheologica Acta*, **1994**, 33(3): 220-237.

15. Plazek D J, O'Rourke V M. *Journal of Polymer Science Part A-2: Polymer Physics*, **1971**, 9(2): 209-243.
16. Gotro J T, Graessley W W. *Macromolecules*, **1984**, 17(12): 2767-2775.
17. Abdel-Goad M, Pyckhout-Hintzen W, Kahle S, et al. *Macromolecules*, **2004**, 37(21): 8135-8144.
18. Likhtman A E, McLeish T C B. *Macromolecules*, **2002**, 35(16): 6332-6343.

Chapter 4 Nonlinear Shear and Elongational Rheology of PPC

4.1 Introduction

The nonlinear viscoelasticity (NLVE) of PPC has been rarely reported and it has not been systematically investigated. One may argue that the viscoelastic parameters determined in Chapter 3 are sufficient to describe the viscoelasticity even in the nonlinear range owing to the success of molecular theories like tube models. However, as mentioned in Chapter 1, these theories rely on the universal behavior of polymers, and recent experiments have revealed that the universality does not hold for some nonlinear rheological properties. For instance, in recent years, uniaxial elongational studies have also been reported to several polymers[1-3] such as polystyrene (PS) and polyisoprene (PI). Interestingly, unlike shear measurements, uniaxial elongational rheological properties of polymer melts show some polymer species dependence. To explain the discrepancy of elongational data among different polymers, the flow-induced friction reduction assumption was proposed.[4,5] Yaoita et al.[6] examined the friction reduction with experimental elongational viscosity of PS melt and primitive chain network and finite extensibility (PCN-FENE) model simulation. Masubuchi et al.[7] successfully predicted the elongational viscosity of PS and PI by PCN-FENE considering friction reduction. However, for poly(n-butyl acrylate) (PnBA), the data is described by simulation result without friction reduction. The friction reduction effect is not universal and needs to be examined for more polymer species.

NLVE properties of PPC are still not understood. The purpose of Chapter 4 is to investigate the nonlinear shear and elongational rheological properties of PPC samples having different molecular weights with relatively narrow molecular weight distributions. Startup shear and uniaxial elongational measurements were conducted for the PPCs at various strain rates and temperatures and were compared with reported polymers. The uniaxial elongational behaviors for PPC were quantitatively compared

with PS. In addition, the experimental data were analyzed through PCN-FENE simulations with the friction reduction.

4.2 Experiments

4.2.1 Samples

Six PPC samples (i.e., PPC344k, PPC253k, PPC158k, PPC111k, PPC95.3k, and PPC68.8k) prepared and characterized in Chapter 2 were used. One PS sample (PS520k, explained in Chapter 2) was used as a reference for comparison of the nonlinear elongational behavior with PPC158k, which possesses similar Z and M_w/M_n values.

Here, a characteristic disengagement relaxation time, τ_d, of the PPCs is defined as the reciprocal of ω at the cross point of G' and G'' in the terminal region. In this study, τ_d, instead of τ_w (the weight-average relaxation time), is used because it is insensitive to the molecular weight distribution. τ_e is a characteristic entanglement relaxation time, defined as the reciprocal of ω at the cross point of G' and G'' in the transition region. All the values estimated are summarized in Table 4.1.

Table 4.1 Entanglement number and characteristic time for PPC and PS

Sample	M_w (kg/mol)	Z [a]	τ_d (s) [b]	$10^5\,\tau_e$ (s) [c]
PPC344k	344	58	121	4.7
PPC253k	253	43	34	3.6
PPC158k	158	27	6.7	3.6
PPC111k	111	19	1.5	3.2
PPC95.3k	95.3	16	0.80	2.8
PPC68.8k	68.8	12	0.17	2.2
PS520k	520	29	8.7×10^3	5.6×10^3

[a]Estimated from $Z = M_w/M_e$, M_e=5.9 kg/mol for PPC, M_e = 18.0 kg/mol for PS.

[b,c]Estimated for PPC at 100 °C and for PS at 130 °C.

4.2.2 Measurements

Startup shear tests were conducted using a rheometer MCR301 (Anton-Paar) with a cone-plate geometry. The diameter of the cone plate was 8 mm and the cone angle was 1°. A PPC sample was loaded at high temperature 140 °C and then pressed to the required gap value (0.026 mm) by the cone plate. After torque became zero, temperature was decreased to the test temperature. PPC samples were measured at 90-120 °C at various shear rates $\dot{\gamma}$ in the range of 0.003–100 s^{-1}. The repeatability of the obtained data was tested by measuring several times while loading fresh samples.

Uniaxial elongation tests were performed with a filament-stretching rheometer (FSR), VADER1000 (RheoFilament). PPC samples were molded to cylinder specimens at 120-140 °C by a hot press. The diameter of the samples was 6 mm and the thickness was 2 mm. The PPC samples were loaded on a stainless geometry with a diameter of 6 mm at 120-140 °C, and then pre-stretched to the diameter of 2-3 mm. To avoid the detachment of the sample from the jig, an epoxy glue was attached to the surface of jigs for some samples. Then, the temperature was decreased to that for measurements (i.e., 70-100 °C) depending on the PPC samples. After the axial force became stable, PPC samples were stretched at various constant strain rates $\dot{\varepsilon}$ in the range of 0.002-2 s^{-1}.

4.3 Results and Discussion

4.3.1 Startup Shear Data of PPC

Figure 4.1 shows the transient shear viscosity growth functions $\eta^+(t)$ at different shear rates $\dot{\gamma}$ for six fractionated PPC samples. The viscosity datasets in Figures 4.1(a-b) were measured at 120 °C, while those in Figures 4.1(c-f) were at 100 °C. When $\dot{\gamma}$ is low, $\eta^+(t)$ for the fractionated PPCs can coincide with LVE curves, although some show small deviation. (A cone-shaped jig used in this study has a radius R_c of 4 mm, a specified gap h of 0.026 mm, and a cone angle α of 1°. The radius of truncated cone is calculated as $R_T = h/\tan\alpha = 0.026/\tan 1° = 1.49$ mm. The error of the shear stress was estimated as $R_T/R_c = 1.49/4 = 37\%$.)

When $\dot{\gamma}$ increases, $\eta^+(t)$ over the entire measurement time clearly decreases, which is known as shear thinning, and a stress overshoot occurred before reaching the steady state, which is common for many reported entangled polymers.[8,9] The molecular origin of this stress overshoot at high $\dot{\gamma}$ is considered to be due to the chain orientation along the flow direction.[10,11] At high $\dot{\gamma}$, the tests were repeated several times with fresh samples, however, the edge fracture is difficult to be completely avoided.[12]

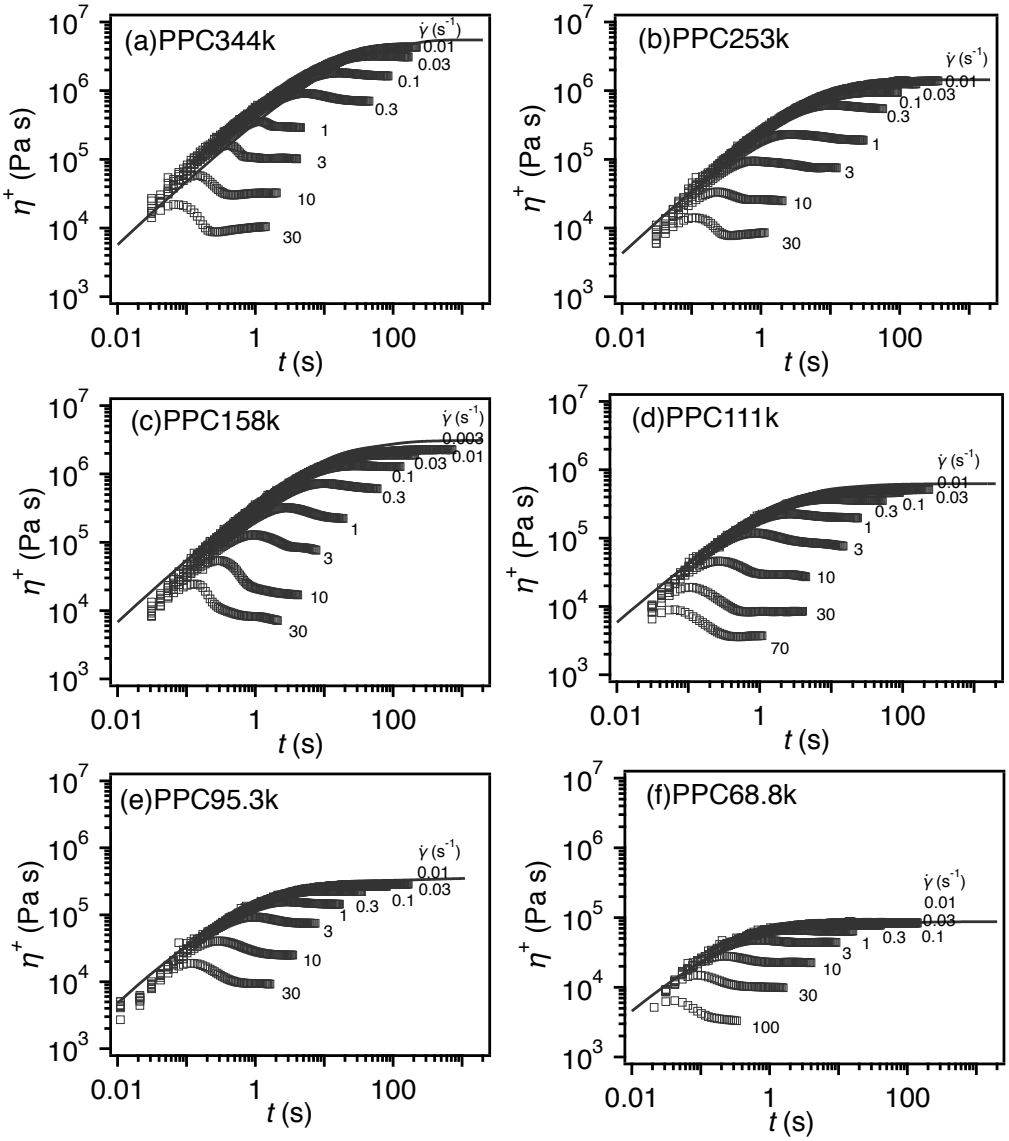

Figure 4.1 Transient shear viscosity η^+ against time t at different shear rates $\dot{\gamma}$ for six PPC samples measured at (a)-(b) 120 °C, and (c)-(f) 100 °C.

Figure 4.2 shows the transient shear viscosities for PPC111k under various $\dot{\gamma}$ at different temperatures, and the data are reduced at the reference temperature T_r = 100 °C. The shear viscosity data measured at 90 °C and 95 °C were shifted to those at 100 °C using both a_T and b_T reported in Chapter 3, where a_T = 1.0, 1.8 and 3.6, and b_T = 1.0, 1.03 and 1.07, at 100, 95 and 90 °C, respectively. Here, the vertical shift factor b_T was used for nonlinear shear data to be comparable with the LVE data. At the same Weissenberg number Wi_d ($= \dot{\gamma}\tau_d$), the viscosity data at different temperatures show a good agreement within an error, indicating that the empirical time-temperature superposition (tTS) is applicable for the PPCs even for nonlinear shear data. This experimental fact has also been reported in previous research for other polymers such as PS,[9], PI,[13] and LDPE.[14]

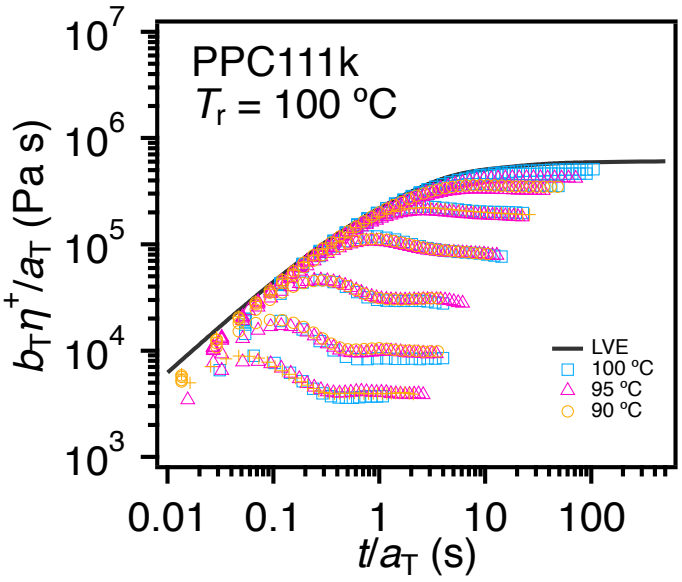

Figure 4.2 Transient shear viscosity η^+ at different $\dot{\gamma}$ for PPC111k at T_r = 100 °C using a_T and b_T. W_{id} = 0.046, 0.46, 1.4, 4.6, 15.4, 46.2, and 108 from top to bottom.

4.3.2 Steady-State Shear Viscosity of PPC

Figure 4.3 plots the steady-state shear viscosity η against $\dot{\gamma}$ and the complex viscosity $\eta^*(\omega)$ against ω at T_r = 100 °C. Shear data for PPC344k and PPC253k were shifted from 120 °C to 100 °C using a_T (= 0.12) and b_T (= 0.88) in the same manner as explained in Figure 4.2.

At low $\dot{\gamma}$, $\eta(\dot{\gamma})$ increases with increasing the molecular weight of PPCs. This result is consistent with the results of the LVE in Chapter 2. At high $\dot{\gamma}$, $\eta(\dot{\gamma})$ for the PPCs are decreased sharply and they are superimposed to a single line with a slope of −0.94 irrespective of the molecular weight. $\eta(\dot{\gamma})$ coincides with $\eta^*(\omega)$, following the empirical Cox-Merz rule ($\eta(\dot{\gamma}) = \eta^*(\omega)|_{\omega=\dot{\gamma}}$),[15] which is known to be valid for many other polymers. Although the fractionated PPC samples have a slightly broad distribution (i.e., M_w/M_n = 1.3-1.4), the Cox-Merz rule is not violated, as known for the broad molecular weight distribution samples.[9] When carefully looking at the data, the steady-state viscosity shows a slightly lower value than the corresponding complex viscosity at high $\dot{\gamma}$. One possible reason is the edge fracture.[12] Snijker et al.[16] reported a cone-partitioned-plate geometry (CPP) to measure the nonlinear startup shear of several polymer melts such as PS and PI to avoid the edge fracture. However, both PI and PS show slightly lower viscosities than the complex viscosities at high $\dot{\gamma}$ when $Wi_d > 1$ in both conventional cone-plate and CPP geometries.

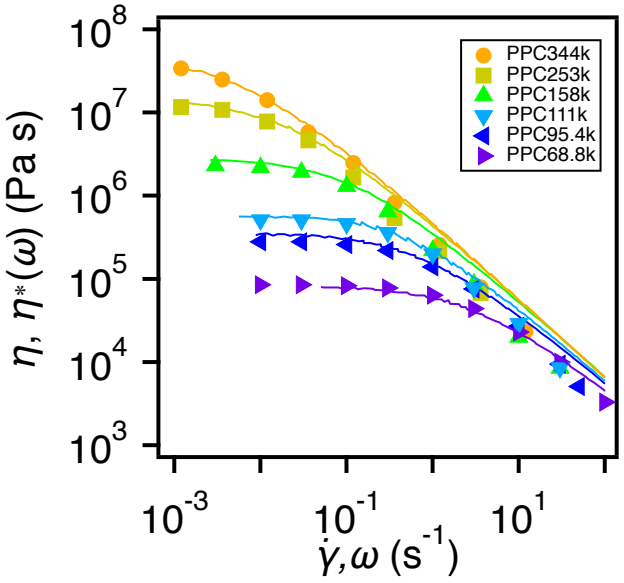

Figure 4.3 Steady-state shear viscosity η against shear rate $\dot{\gamma}$ for fractionated PPCs. The data of PPC344k and PPC253k are shifted from 120 °C to 100 °C using a_T and b_T. The solid curves are the complex viscosity $\eta^*(\omega)$ from dynamic measurement.

Figure 4.4 shows the steady-state shear viscosities normalized by the zero-shear viscosity η_0 as a function of $\dot{\gamma}\tau_d$, for PPC (filled symbols) compared with other polymers. The data of PS (unfilled black triangle), PI (unfilled black circle) are taken from Snijker et al.[16] After the normalization, the experimental data for PPC can be compared with other polymers. From Figure 4.4 the data for PPC are in good agreement with PS and PI, independent of molecular weight and polymer species. Consequently, nonlinear shear data of PPC follows the universality.

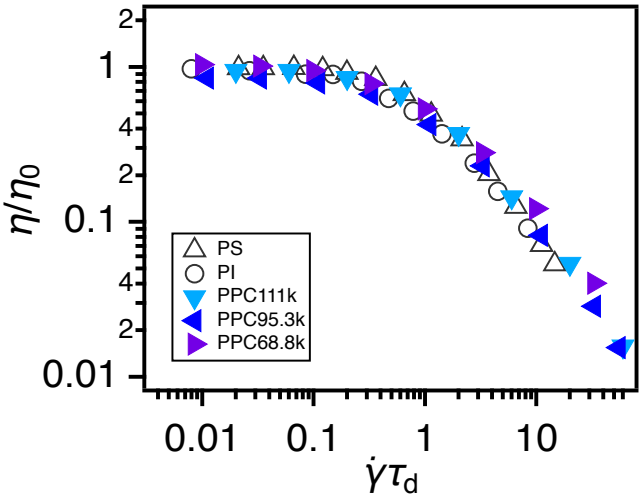

Figure 4.4 Normalized steady-state shear viscosity of PPC. The data of PS and PI are taken from literature with permisssion.[16]

4.3.3 Dependence of Stress Maximum of Shear Rate

As explained in Figure 4.1, the PPC samples exhibit a stress overshoot of the transient viscosity at high $\dot{\gamma}$. Figure 4.5 shows the maximum strain γ_{max} plotted against Wi_d ($= \dot{\gamma}\tau_d$), where γ_{max} is defined as $\dot{\gamma}t_{max}$ (t_{max} is a time at the maximum viscosity of the stress overshoot). When Wi_d is small (<1), the γ_{max} value is around 2. Although high $\dot{\gamma}$ was not examined in this study, the maximum strain increases with increasing $\dot{\gamma}$ with power-law manner with the exponent of 1/3. This scaling phenomenon is reported for several polymers such as PS, PI,[17] styrene-butadiene rubber (SBR),[18] and polybutadiene (PBD).[19] In addition, the constant maximum strain (≈ 2) at small shear rate and $\gamma_{max} \sim \dot{\gamma}\tau_d{}^{1/3}$ at large shear rates has been predicted by simulations.[20,21]

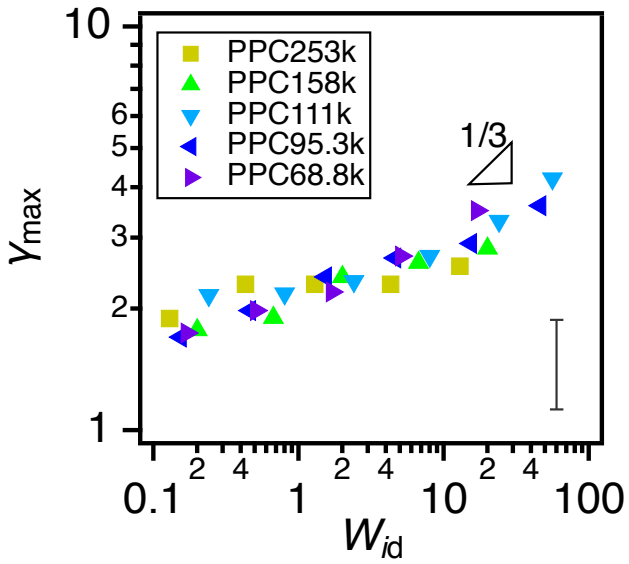

Figure 4.5 The maximum strain $\gamma_{\max}$ as a function of Wi_{d} for PPC.

4.3.4 Elongational Data of PPC

Figure 4.6 shows the transient elongational viscosity $\eta_{\mathrm{E}}^{+}(t)$ at various elongational rates $\dot{\varepsilon}$ for the fractionated PPCs. When $\dot{\varepsilon}$ is small, $\eta_{\mathrm{E}}^{+}(t)$ follows the LVE envelopes for most of the PPCs. Here, the LVE envelopes are calculated from master curves of G' and G'' in Chapter 3 after Fourier transforms as $\eta_{\mathrm{E}}^{+}(t) = 3\int_0^t G(t')dt'$. Note that PPC111k shows a clear deviation of $\eta_{\mathrm{E}}^{+}(t)$ from the LVE, but the reason is unknown. When $\dot{\varepsilon}$ becomes higher, a deviation of $\eta_{\mathrm{E}}^{+}(t)$ from the LVE curve to the higher side at long t is observed for the fractionated PPCs, and then the viscosity reached the steady state, although the steady state was not that wide. Similar phenomena have been reported for some linear polymer melts.[1,3]

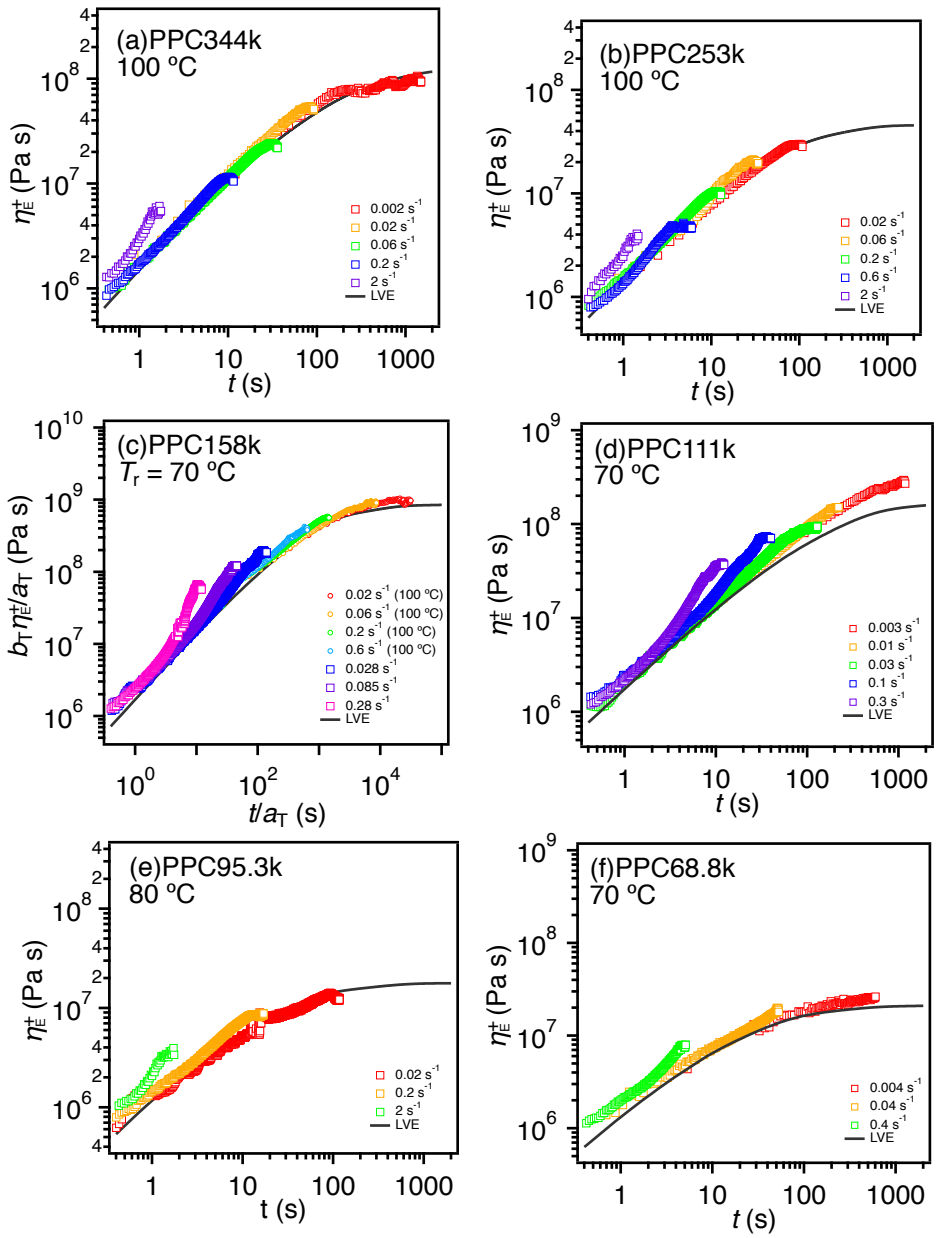

Figure 4.6 Transient elongational viscosity η_E^+ at various elongational rates $\dot{\varepsilon}$ for the fractionated PPCs measured at (a)-(b) 100 °C, (c) (d) (f) 70 °C, and (e) 80 °C.

Figure 4.7 plots $\eta_E^+(t)$ for PPC111k measured at different temperatures, and they are reduced at T_r = 70 °C. The same procedure was performed in shear measurements as explained above as Figure 4.2 with a_T = 1.0, 0.37 and 0.15, and b_T = 1.0, 0.97 and 0.94, at 70, 75 and 80 °C, respectively. As can be seen that $\eta_E^+(t)$ at different temperatures coincide well after adequately shifting the data, tTS can be applicable to PPC in nonlinear elongational behaviors.

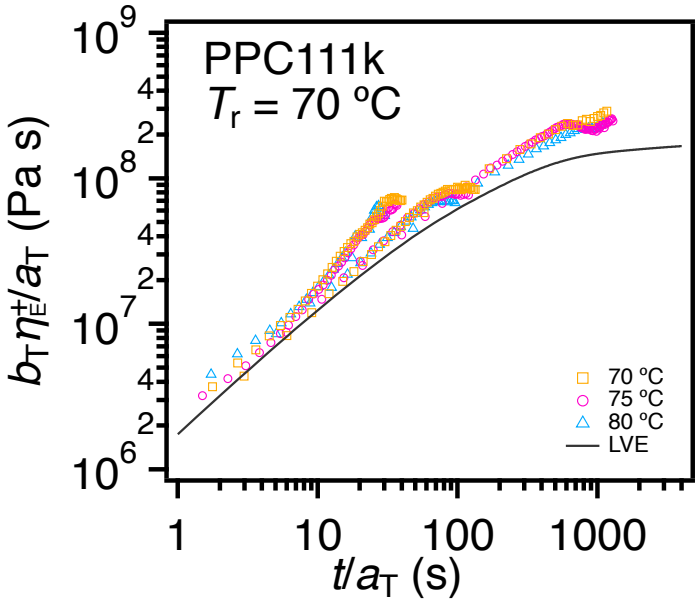

Figure 4.7 Transient elongational viscosity η_E^+ at different elongational rates $\dot{\varepsilon}$ for PPC111k measured at different temperatures reduced at T_r = 70 °C using a_T and b_T. W_{id} = 0.42, 4.2 and 14 from right to left.

4.3.5 Steady-State Elongational Viscosity of PPC

Figure 4.8 shows the transient stress against the Hencky strain at various $\dot{\varepsilon}$ for the fractionated PPCs for the raw data are shown in Figure 4.6. As can be seen, the stresses for the PPC samples at various $\dot{\varepsilon}$ increase with the Hencky strain and finally reach a constant value, which is the so-called steady-state stress. Note that some stress data did not reach a stable steady-state. From Figure 4.8, the steady-state elongational viscosities η_E for the PPCs are estimated from the average value at large Hencky strain region with an error.

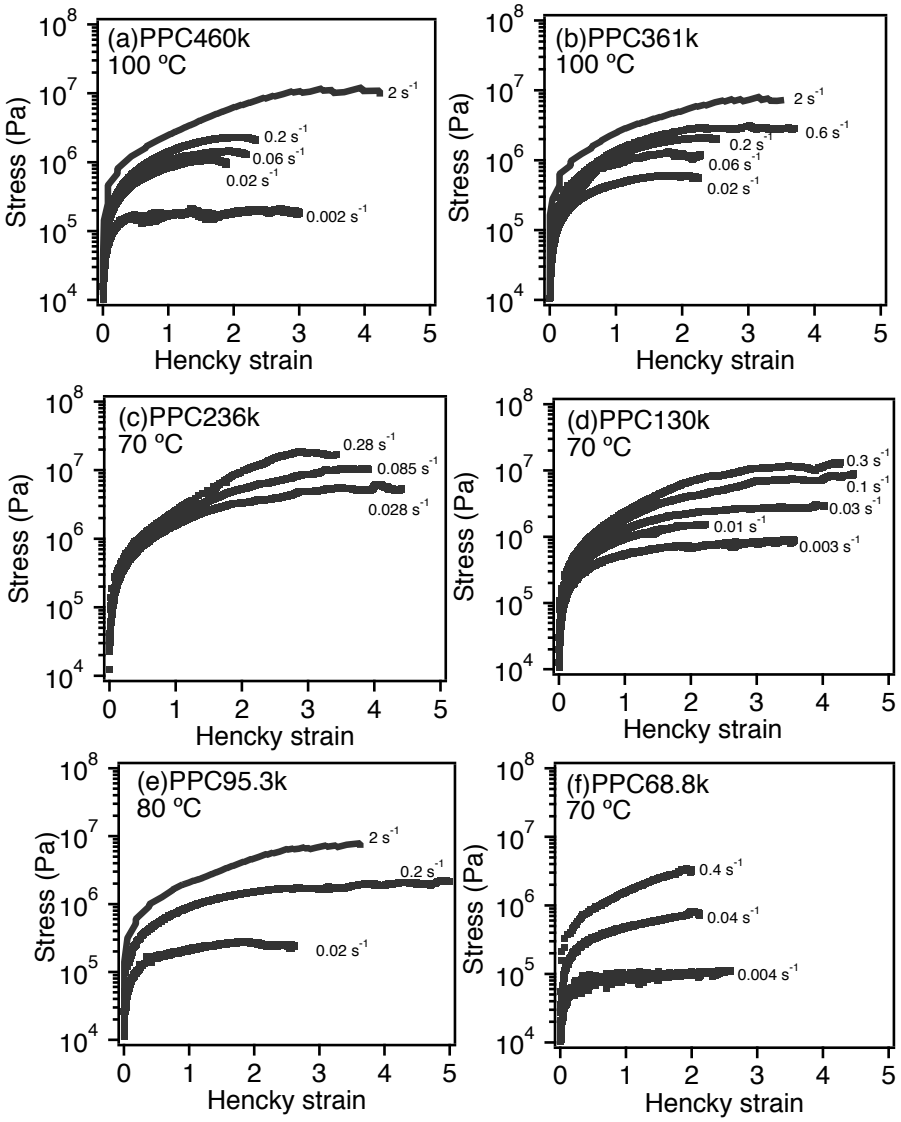

Figure 4.8 Transient stress vs Hencky strain at various elongation rates $\dot{\varepsilon}$ (in linear scale) for the fractionated PPCs.

Figure 4.9 shows the steady-state viscosity η_E against elongational rate $\dot{\varepsilon}$ for PPCs. PPC samples are measured at different temperatures and elongation rates. From Figure 4.9 the elongational viscosity decreases with elongational rate for all PPC samples.

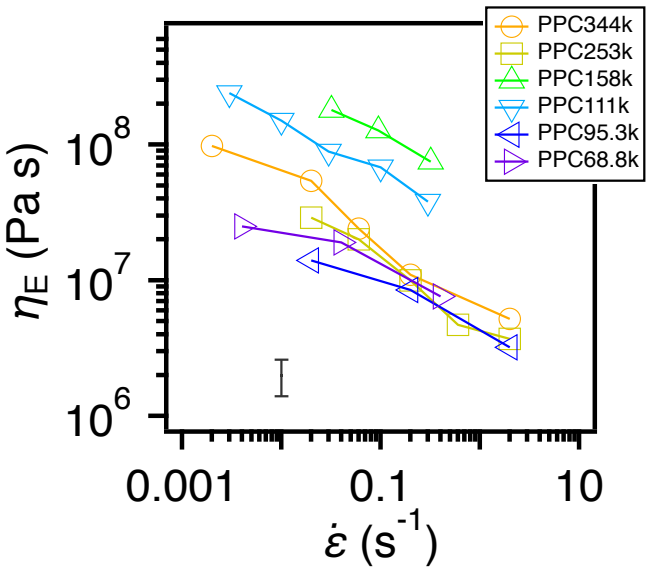

Figure 4.9 Steady-state elongational viscosity $\eta_E(\dot{\varepsilon})$ as a function of elongational rate $\dot{\varepsilon}$ for the fractionated PPCs. The averaged error bar of the data is shown.

Figure 4.10 shows the normalized steady-state viscosity where η_E is divided by $3\eta_0$ and $\dot{\varepsilon}$ multiplied by τ_d as $Wi_d = \dot{\varepsilon}\tau_d$. All the fractionated PPCs follow a power-law decay described as $\eta_E \sim \dot{\varepsilon}^{-0.5}$. This scaling behavior with the power of −0.5 is reported for PS.[22,23]

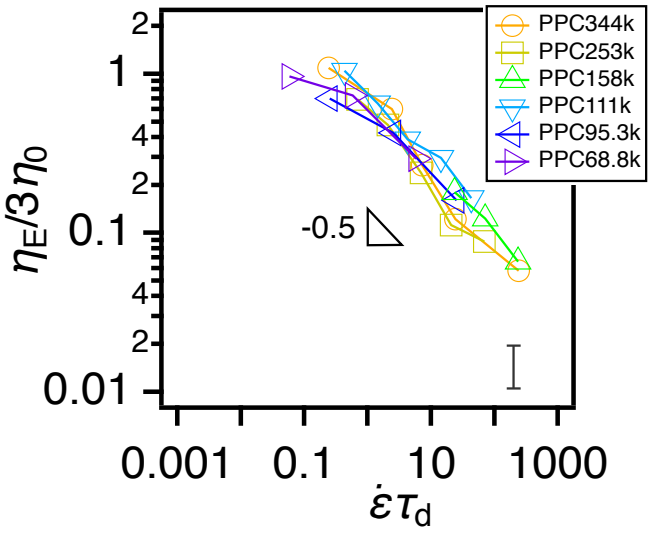

Figure 4.10 Normalized steady-state elongational viscosity $\eta_E(\dot{\varepsilon})/3\eta_0$ as a function of $\dot{\varepsilon}\tau_d$ for the fractionated PPCs.

4.3.6 Estimation of Maximum Stretching Ratio of PPC

To further compare and discuss the elongational data for the PPCs, the characteristic ratio C_∞ and Kuhn segment length l_K of PPC were necessary. The maximum stretching ratio λ_{max} depends on the polymer species, and is considered to influence the elongational behavior especially at high $\dot{\varepsilon}$, based on the tube model with introducing the FENE effect for entangled polymers. Although λ_{max} has been reported for many polymers, λ_{max} of PPC has not been reported, and hence it is estimated based on the packing length concept.[24,25]

The packing length p is defined as:

$$p = M/\{\langle R^2\rangle_0 \rho N_A\} \qquad (4\text{-}1)$$

Here, M is the molecular weight, $\langle R^2\rangle_0$ is the unperturbed mean-square end-to-end distance, ρ is the density, N_A is the Avogadro's number.

According to the data for many polymers, p and G_N^0 follows the relationship:[24]

$$p^3 G_N^0 = 12.16 \text{ MPaÅ}^3 \qquad (4\text{-}2)$$

G_N^0 is estimated as 670 kPa in Chapter 2. The packing length p for PPC is calculated as 2.63 Å.

The characteristic ratio C_∞ follows the expression:

$$C_\infty = (\langle R^2\rangle_0/M)\,(m_0/l_0^2) = m_0/(l_0^2 p \rho N_A) \qquad (4\text{-}3)$$

Here, the molecular weight m_0 is the average molecular weight per backbone bond of length l_0. m_0 is estimated as 20.42 g/mol and l_0 as 1.19 Å for PPC.[26] Hence C_∞ is calculated as 7.22.

The Kuhn segment length l_K and Kuhn segment molecular weight m_K are given by:

$$l_K = C_\infty l_0 = 8.59 \text{ Å} \qquad (4\text{-}4)$$

$$m_K = (1/C_\infty)\, m_0\, (l_K/l_0)^2 = C_\infty\, m_0 = 147 \text{ g/mol} \qquad (4\text{-}5)$$

The number of Kuhn segments in an entanglement segment can be calculated from m_K as (M_e = 5.9 kg/mol for PPC in Chapter 2) :

$$N_e = M_e/m_K = 40.1 \qquad (4\text{-}6)$$

Finally, the maximum stretch ratio can be estimated as:

$$\lambda_{max} = \sqrt{(M_e/m_K)} = 6.3 \qquad (4\text{-}7)$$

4.3.7 Direct Comparison with PS

The elongational behavior of PPC reported above seems very similar to that reported for PS. In this section, direct comparison is attempted for a pair of PS and PPC melts, for which Z and M_w/M_n are almost the same.

Figure 4.11 plots the normalized master curves of G' and G'' for both PPC and PS. PPC158k ($Z = 27$, $M_w/M_n = 1.3$) has a similar Z value and molecular weight distribution with PS520k ($Z = 29$, $M_w/M_n = 1.3$). G' and G'' of PPC158k show a great agreement with those of PS520k in wide ω range including transition regime, plateau regime, and terminal regime by adequately selecting the normalizing parameters. This kind of comparison was successfully conducted for other polymers by Morelly et al.[3] for example. For their case, the normalized master curves of G' and G'' for PS and PMMA coincided well.

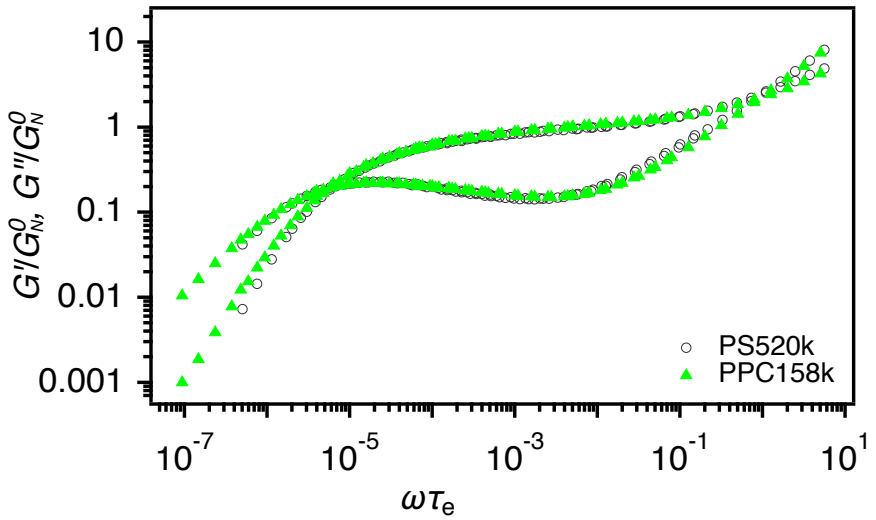

Figure 4.11 Normalized master curves of G' and G'' of PPC236k (filled triangle) and PS520k (open circle) against $\omega\tau_e$.

Figure 4.12 shows the comparison of normalized elongational viscosity against time for PPC158k and PS520k at the same Weissenberg numbers Wi_d = 23.8, 71.5, and 238. Here, PS520k was measured at 0.0028 s^{-1}, 0.0084 s^{-1}, and 0.028 s^{-1} at 130 °C. τ_e values were used from Table 4.1. To directly compare the elongational data for PPC and PS, the elongational data were normalized by the three LVE parameters, i.e., Z, G_N^0 and τ_e. As shown in Figure 4.12, the normalized LVE curves for the PPC and PS coincide well apart from a small deviation at low ω region. The transient elongational viscosity curves for the PPC and PS samples superpose within an experiment error. At two lower Wi_d values, PPC158k reaches higher steady-state viscosities than PS520k. At the highest Wi_d value, PPC158k shows a similar steady-state viscosity with PS520k.

From the FENE model prediction discussed in Chapter 1, λ_{max} determines the elongational behavior of polymers at high Wi_R (> 1) regime. In the previous subsection, λ_{max} of PPC was estimated as 6.3, while that of PS is reported as 4.7.[22] The λ_{max} value of PPC (= 6.3) is somewhat higher than PS (= 4.7), however, PPC158k and PS520k show overlapped elongational viscosity curves at very high Wi_d. This result implies that η_E is not dominated by λ_{max}.

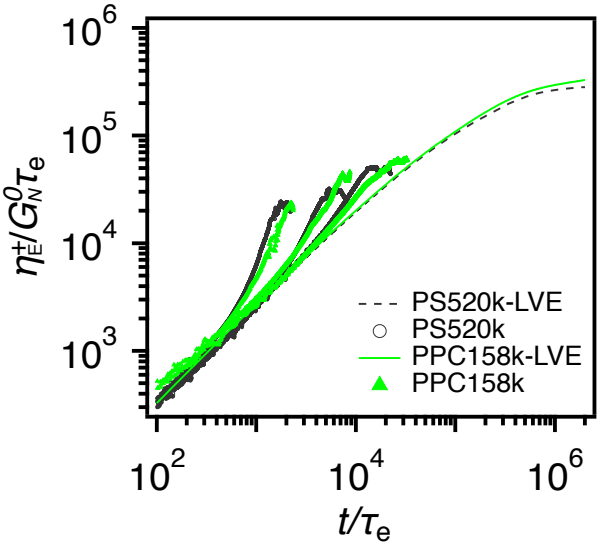

Figure 4.12 Normalized elongational viscosity $\eta_E^+/G_N^0\tau_e$ against t/τ_e for PPC158k and PS520k at the same Wi_d. The detailed Wi_d values are shown in the panel.

Figure 4.13 plots the normalized steady-state elongational viscosity, i.e., η_E normalized by $3\eta_0$, against $\dot{\varepsilon}\tau_d$ for PPC158k and PS520k. It is obvious that the steady-state viscosities decrease with increasing $\dot{\varepsilon}\tau_d$, and the normalized η_E values at the same $\dot{\varepsilon}\tau_d$ are very close to each other for PPC and PS within an error. The Rouse Weissenberg number $\dot{\varepsilon}\tau_R$ is normally used to characterize the chain stretch in previous studies. However, the Rouse relaxation time τ_R is difficult to estimate for PPC and PS because of their broad M_w/M_n (= 1.3). Nevertheless, an estimate of τ_R can be given by $\tau_R/3Z$ so that the chain stretch is assumed to be induced around $\dot{\varepsilon}\tau_d \sim 90$. But no sign of upturn is observed. One possible reason for the absence of viscosity upturn may be due to the friction reduction happening when chains are highly stretched and oriented, as discussed in Appendix.

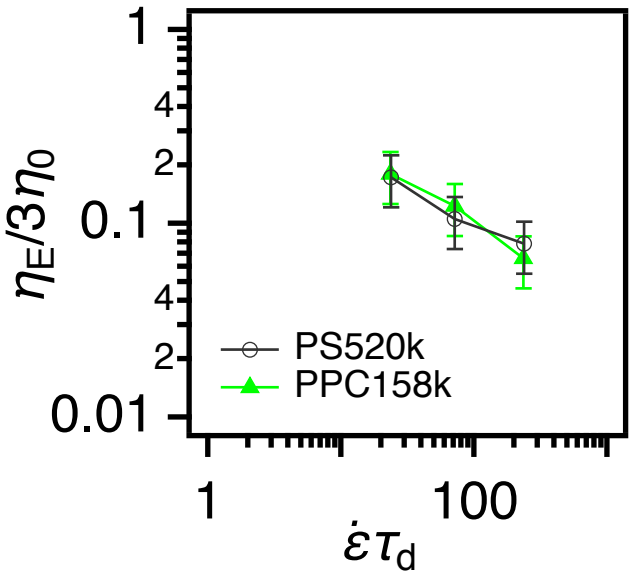

Figure 4.13 Normalized steady-state elongational viscosity $\eta_E(\dot{\varepsilon})/3\eta_0$ as a function of $\dot{\varepsilon}\tau_d$ for PPC158k compared with PS520k.

4.3.8 Comparison with Other Reported Polymers

Figure 4.14 shows the normalized steady-state elongational viscosity as a function of normalized elongational rate for PPC and other reported polymer melts PI, PnBA by Sridhar et al.[2] and PS, PMMA, PtBS by Morelly et al.[3]. The data taken from literature

for other polymers are recalculated by τ_d, the reciprocal of frequency at the cross point of G' and G'' in the terminal region to set the index of τ_d with the present study. As predicted in the tube theory discussed in Chapter 1, the position of viscosity upturn is related to the Rouse relaxation rate, and thus, this comparison is meaningful only when Z is common for all the cases. Z values are 19/27/58 for PPC, 29 for PI, 13 for PnBA, 20 for PS, 20 for PMMA, 10 for PtBS. Even with this difference of Z, except PnBA, no viscosity upturn is observed, implying that the friction reduction occurs for most of polymers. Earlier studies argued that polymers with side chains may be less affected by friction reduction. PPC has no bulky side chains and does not show an upturn of η_E at high $\dot{\varepsilon}$, which follows the previous assumption.

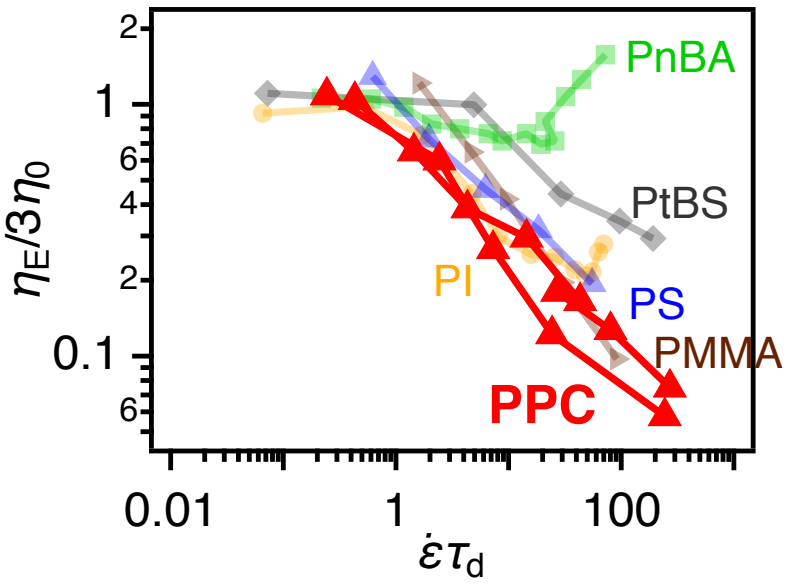

Figure 4.14 Normalized steady-state elongational viscosity $\eta_E(\dot{\varepsilon})/3\eta_0$ as a function of $\dot{\varepsilon}\tau_d$ for PPCs and other reported polymer melts where the data are taken from literature in Refs. 2 and 3.

4.4 Conclusion

The nonlinear shear and elongational rheological properties of fractionated PPCs were investigated. For shear experiments, transient shear viscosities of PPC decreased with increasing shear rates, and they were lower than LVE curves when $\dot{\varepsilon}\tau_d > 1$. Steady-

state shear viscosities showed good agreement with dynamic viscosities, following the empirical Cox-Merz rule. These results were consistent with the results reported for other polymers. For uniaxial elongation measurements, transient elongational viscosities of the PPCs increased with increasing elongation rates, and they were slightly deviated from the LVE curves to the higher side at high elongation rates. This result is similar to some other polymer melts such as polystyrene. Steady-state elongational viscosities decreased with increasing elongation rates for all PPC samples with a slope of −0.5, which was similar to the PS data. In addition, the elongational data of PPC were directly compared with PS with similar Z and M_w/M_n values. The normalized elongational viscosities at the same Weissenberg number $\dot{\varepsilon}\tau_d$ for PPC and PS were similar to each other within an error. The normalized steady-state elongational viscosities for PPC showed similar values with PS at the same $\dot{\varepsilon}\tau_d$. Despite that PPC had a slightly higher λ_{max} value than PS, PPC and PS samples showed similar elongational behaviors, which may be due to the monomeric friction reduction.

4.5 References

1. Bach A, Almdal K, Rasmussen H K, et al. *Macromolecules*, **2003**, 36(14): 5174-5179.
2. Sridhar T, Acharya M, Nguyen D A, et al. *Macromolecules*, **2014**, 47(1): 379-386.
3. Morelly S L, Palmese L, Watanabe H, et al. *Macromolecules*, **2019**, 52(3): 915-922.
4. Ianniruberto G, Brasiello A, Marrucci G. *Macromolecules*, **2012**, 45(19): 8058-8066.
5. Ianniruberto G, Marrucci G, Masubuchi Y. *Macromolecules*, **2020**, 53(13): 5023-5033.
6. Yaoita T, Isaki T, Masubuchi Y, et al. *Macromolecules*, **2012**, 45(6): 2773-2782.
7. Masubuchi Y, Matsumiya Y, Watanabe H. *Macromolecules*, **2014**, 47(19): 6768-6775.

8. Ferry JD, "*Viscoelastic Properties of Polymers*", 3rd ed, (**1980**), John Wiley & Sons Inc, New York.
9. Graessley WW. "*Polymeric Liquids & Networks: Dynamics and Rheology*", (**2008**), Garland Science, London and New York.
10. Masubuchi Y, Watanabe H. *ACS Macro Letters*, **2014**, 3(11): 1183-1186.
11. Jeong S, Kim J M, Baig C. *Macromolecules*, **2017**, 50(8): 3424-3429.
12. Parisi D, Han A, Seo J, et al. *Journal of Rheology*, **2021**, 65(4): 605-616.
13. Auhl D, Ramirez J, Likhtman A E, et al. *Journal of Rheology*, **2008**, 52(3): 801-835.
14. Laun H M. *Rheologica Acta*, **1978**, 17(1): 1-15.
15. Cox W P, Merz E H. *Journal of Polymer Science*, **1958**, 28(118): 619-622.
16. Snijkers F, Vlassopoulos D. *Journal of Rheology*, **2011**, 55(6): 1167-1186.
17. Schweizer T. *Journal of Rheology*, **2003**, 47(4): 1071-1085.
18. Boukany P E, Wang S Q, Wang X. *Journal of Rheology*, **2009**, 53(3): 617-629.
19. Ravindranath S, Wang S Q. *Journal of Rheology*, **2008**, 52(3): 681-695.
20. Xie S J, Schweizer K S. *Macromolecules*, **2018**, 51(11): 4185-4200.
21. Becerra D, Córdoba A, Schieber J D. *Macromolecules*, **2021**, 54(17): 8033-8042.
22. Huang Q, Mednova O, Rasmussen H K, et al. *Macromolecules*, **2013**, 46(12): 5026-5035.
23. Narimissa E, Poh L, Wagner M H. *Rheologica Acta*, **2021**, 60(4): 163-174.
24. Fetters L J, Lohse D J, Richter D, et al. *Macromolecules*, **1994**, 27(17): 4639-4647.
25. Fetters L J, Lohse D J, Milner S T, et al. *Macromolecules*, **1999**, 32(20): 6847-6851.
26. Wu S. *Polymer Engineering & Science*, **1992**, 32(12): 823-830.
27. Wingstrand S L, Alvarez N J, Huang Q, et al. *Physical Review Letters*, **2015**, 115(7): 078302.

Chapter 5 Summary

In this thesis, a series of PPC samples with different molecular weights (M_w = 344-68.8 kg/mol) and relatively narrow distributions (M_w/M_n =1.3-1.4) were prepared by fractionation. The linear and nonlinear rheological properties of PPC were studied.

In chapter 1, the background of CO_2-based polycarbonate PPC was introduced. From previous studies on polymer rheology, linear and nonlinear shear rheology of polymer melts are universal but nonlinear uniaxial elongational rheology seems to depend on polymer chemistry. By the limit of previous rheological studies on PPC, the importance of studying both linear and nonlinear rheology of PPC with well-characterized samples was explained.

In chapter 2, the sample preparation and characterization of PPC used for the careful rheological measurements in the thesis were explained. We prepared six PPC samples with relatively narrow molecular weight distribution by fractionation precipitation method, which covered a wide molecular range. The PPC samples were characterized by several methods such as NMR, GPC, MALS, and DSC.

In chapter 3, linear viscoelasticity of fractionated PPCs was investigated. After obtaining the master curves of G' and G'' of PPCs by tTS, several linear parameters were estimated from them and compared with other polymers. The average plateau modulus G_N^0 of PPCs was estimated as 670 kPa, and M_e as 5.9 kg/mol. The obtained G_N^0 value of PPC was compared with previous studies, the values were 0.15 MPa by Lin et al., 0.18 MPa by Ning et al., and 0.3-0.7 MPa by Cao et al. The discrepancy may be due to the commercial samples used in previous studies and different estimation methods. The zero-shear viscosity η_0 and the weight average molecular weight M_w of fractionated PPCs followed the relationship of $\eta_0 \propto M_w^{3.4}$. The linear viscoelastic parameters of PPC samples were compared to other reported polymers such as PS. The results showed that the data obtained in the thesis coincide well with previous data. In

addition, experimental results were compared with LM model prediction. They showed a good agreement apart from the broadening of the viscoelastic spectrum in the terminal zone due to M_w/M_n.

In chapter 4, nonlinear shear and elongational rheological behaviors of fractionated PPCs were investigated. Empirical tTS principle used in LVE was applicable also for nonlinear shear and elongation. For shear, PPC showed shear thinning behavior, that is, shear viscosity decreased with increasing shear rate. Empirical Cox-Merz rules between dynamic viscosity and steady-state viscosity were not violated. For elongation, PPC showed weak strain hardening, that is, transient elongational viscosity deviated from LVE and showed higher curves. The steady-state elongational viscosity for PPC decreased with increasing elongation rate with a power-law manner with the exponent of -0.5. In addition, the elongational behaviors for PPC and PS were compared with similar Z value and similar M_w/M_n = 1.3. The normalized transient elongational viscosity at the same Weissenberg number $\dot{\varepsilon}\tau_d$ for PPC and PS coincides with each other. The normalized steady-state elongational viscosity for PPC decreased with increasing elongational rate similar to PS within an error. PPC was found to behave similar to PS, PI, and PMMA, but is different from PtBS and PnBA, which may be due to the friction reduction under fast elongation.

Throughout this thesis, it has been studied that PPC follows the universal behaviors in linear and nonlinear shear flow, whereas it shows monotonical elongational viscosity decrease with increasing elongational rate which is ascribed to the friction reduction. The linear and nonlinear rheological properties of PPC are similar to PS, PI, and PMMA, but different from PtBS and PnBA.

Appendix

A. Simulation for Elongational Viscosity

A.1 Method

As discussed in section 4.3, PPC behaves similarly to PS under examined uniaxial elongations, implying that PPC exhibits a reduction of monomeric friction as discussed for PS. This conclusion is drawn from the absence of upturn in the steady-state elongational viscosity plotted against strain rate. However, the sample polydispersity does not allow us to specify the critical elongational rate for the upturn, and thus, one may argue that the examined elongational rates are not sufficiently large. Besides, the effect of λ_{max} is also unclear from the experimental data. To clarify these issues, primitive chain network simulations were performed as explained below.

Multi-chain slip-link simulations were conducted for PPC158k and PS520k based on the primitive chain network (PCN) model.[1-4] In the simulation, entangled polymer chains are replaced by a slip-link network. The system consists of network nodes, strands, and dangling ends. Each polymer chain is represented by a path connecting two dangling ends through some network nodes and strands. The position of slip-links and dangling ends follow the Langevin equation of motion. The monomer number distributed on each strand changes with time by the change rate equation. For both equations, four forces, the drag force, the balance of tension of the strands, the osmotic force suppressing the density fluctuation, and the random force, are taken into account. Besides, slip-links are created and destructed at the chain ends according to the monomer number on the dangling ends. The average strand length a, the thermal energy k_BT, and the diffusion time of a single network node $\tau_0 = 2n_0\zeta_0a^2/6k_BT$ are the units of length, energy, and time. Here, ζ_0 is the friction coefficient of the Kuhn segment under equilibrium, and n_0 is the average number of Kuhn segments on the single network strand. λ_{max} is determined from n_0. To reproduce the experiments, unit of molecular weight M_0 and unit of modulus are used instead of a, k_BT, and n_0. The

employed values are (G_0, M_0, λ_{max}, τ_0) = (0.55 MPa, 1.1 kg/mol, 3.9, 1.3 s) for the PS melt at T =130 °C, and (G_0, M_0, λ_{max}, τ_0) = (1.9 MPa, 3.3 kg/mol, 4.9, 0.078 s) for the PPC melt at T = 70 °C. The polydispersity was considered with a log-normal distribution. The friction change was introduced with the model proposed by Iannirubert et al.[5,6]

A.2 Simulation Results

Figure A1 and A2 exhibit transient and steady-state elongational viscosities shown in Figures 4.12 and 4.13 with the simulation results. The simulation reasonably reproduces the experiments both for PS and PPC when the friction is changed. As shown by the broken curves, if constant friction is employed, the steady-state viscosity shows the upturn and the simulation largely overestimates the data.

For the case with the constant friction, due to the difference of λ_{max}, the value $\eta_E/3\eta_0$ for PPC is larger than that for PS in the high stretch rate limit. Nevertheless, the simulation demonstrates that the elongation data cannot be explained without the change of friction, both for PS and PPC.

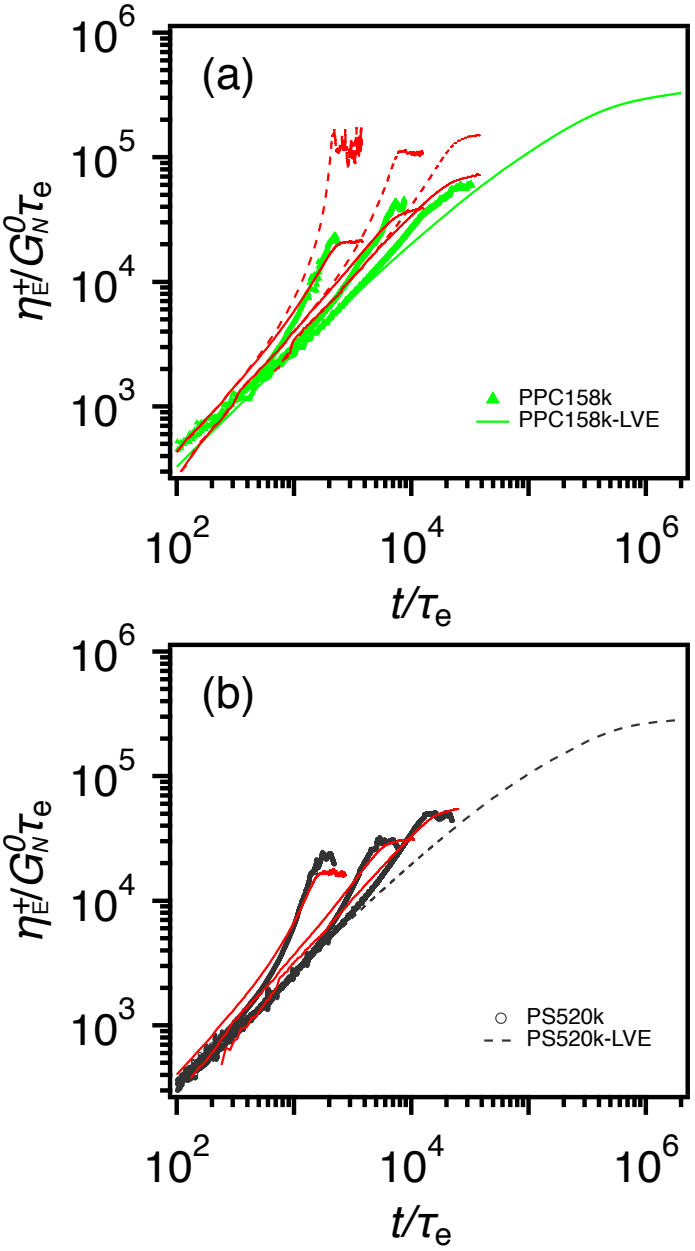

Figure A1 Transient elongational viscosity for (a) PPC158k at $T = 70$ °C and (b) PS520k at $T = 130$ °C. Experimental data are shown by symbols. Simulation results with and without the change of friction are indicated by red solid and broken curves.

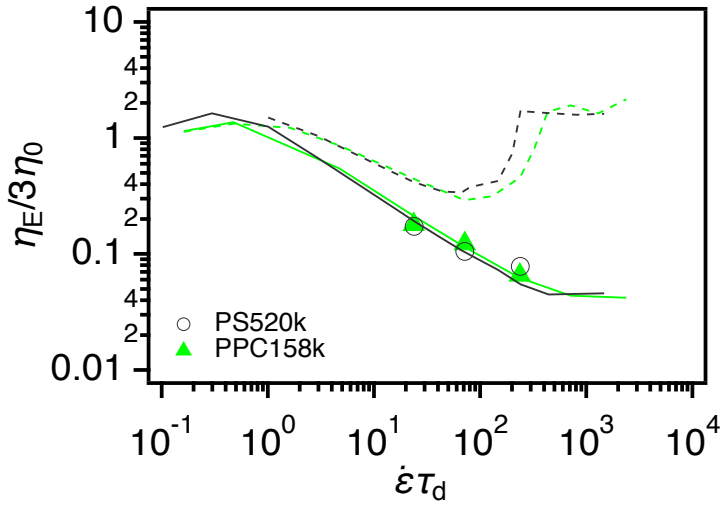

Figure A2 Steady-state elongational viscosity for PPC158k at T = 70 °C and PS520k at T = 130 °C. Experimental data are shown by symbols. Simulation results with and without the change of friction are indicated by solid and broken curves.

A.3 References

1. Masubuchi Y, Takimoto J I, Koyama K, et al. *The Journal of Chemical Physics*, **2001**, 115(9), 4387–4394.
2. Masubuchi Y, Ianniruberto G, Greco F, et al. *Modelling and Simulation in Materials Science and Engineering*, **2004**, 12(3), S91–S100.
3. Masubuchi Y. *Annual Review of Chemical and Biomolecular Engineering*, **2014**, 5, 11–33.
4. Peterlin, A. *The Journal of Chemical Physics*, **1960**, 33, 1799.
5. Ianniruberto G. *Macromolecules*, **2015**, 48(17): 6306-6312.
6. Ianniruberto G, Brasiello A, Marrucci G. *Macromolecules*, **2012**, 45(19): 8058-8066.

List of Publications

1. Lixin Yang, Takashi Uneyama, Yuichi Masubuchi and Yuya Doi, "Linear Rheological Properties of Poly(Propylene Carbonate) with Different Molecular Weights", *Nihon Reoroji Gakkaishi* (*J. Soc. Rheol. Jpn.*), **2021**, 49, 267-274.

2. Lixin Yang, Takashi Uneyama, Yuichi Masubuchi and Yuya Doi, "Nonlinear Shear and Elongational Rheology of Poly(Propylene Carbonate)", *Nihon Reoroji Gakkaishi* (*J. Soc. Rheol. Jpn.*), in press.

3. Lixin Yang, Takashi Uneyama, Yuichi Masubuchi and Yuya Doi, "Linear Rheological Properties of Poly(Propylene Carbonate)-Discussed on Absolute Molecular Weight", in preparation.

4. Lixin Yang, Takashi Uneyama, Yuichi Masubuchi and Yuya Doi, "Direct Comparison of Uniaxial Elongational Rheology of PPC and PS with Same Entanglement Number and Molecular Weight Distribution", in preparation.

Other Publications

5. Yuichi Masubuchi, Lixin Yang, Takashi Uneyama and Yuya Doi, "Primitive Chain Network Simulations for Non-Linear Viscoelasticity of Poly(Propylene Carbonate) Melt", *Polymers*, submitted.

Conferences

1. 楊麗欣，木田拓充，土肥侑也，畝山多加志，増渕雄一, “Nonlinear shear and elongational rheology of poly(propylene carbonate)”, 日本レオロジー学会第 48 年会(2021/5/13-14)講演番号 12, オンライン, 口頭発表.
2. Lixin Yang, Yuya Doi, Takashi Uneyama and Yuichi Masubuchi, “Uniaxial elongational flow of different poly(alkylene carbonate)”, The 21st International

Union of Materials Research Societies – International Conference in Asia (IUMRS-ICA2020), (2021.2.23-26)R1_O17, Thailand, online, oral.

3. 楊麗欣，土肥侑也，畝山多加志，増渕雄一，”Nonlinear elongational rheology of poly(propylene carbonate)”，第 13 回西日本支部学生ワークショップ(2020/10/23)発表 4，オンライン，口頭発表.
4. 楊麗欣，土肥侑也，畝山多加志，増渕雄一，”Stress relaxation after uniaxial elongation of PPC melts”，第 69 回高分子討論会(2020/9/16-18)PB3b01，オンライン，ポスター発表.
5. Lixin Yang, Takashi Uneyama and Yuichi Masubuchi, “Uniaxial Elongational Viscosity of Poly(Propylene Carbonate)”, The 15thInternational Workshop for East Asian Young Rheologists(2020.1.8-11)L03, Changchun, China, oral.
6. Lixin Yang, Takashi Uneyama and Yuichi Masubuchi, “Non-linear rheological behaviors of poly(propylene carbonate)”, 第 67 回レオロジー討論会(2019/10/16-18)3C05, 彦根, 口頭発表.
7. Lixin Yang, Takashi Uneyama and Yuichi Masubuchi, “The effect of molecular weight distributions on the rheological properties of poly(propylene carbonate)”, Polymer Engineering and Science International Conference(2019/9/4-7)P023, 米沢, ポスター発表.
8. Lixin Yang, Takashi Uneyama and Yuichi Masubuchi, “Linear viscoelastic parameters of Poly(Propylene Carbonate) with different molecular weight and distributions”, 日本レオロジー学会第46年会(2019/5/8-9)P33, 京都, ポスター発表.
9. Lixin Yang, Tetsuya Yamamoto, Takashi Uneyama and Yuichi Masubuchi, “Rheological Properties of Poly(Propylene Carbonate) and Modeling”, The 14th International Workshop for East Asian Young Rheologists(2019/1/23-26)P04, 名古屋, ポスター発表.

Acknowledgement

This thesis was carried out at Department of Materials Physics, Graduate School of Engineering, Nagoya University. The work was conducted under the supervision of Professor Masubuchi Yuichi during the period from October 2018 to March 2022. This doctor project was funded by China Scholarship Council (No. 201809110142).

I would like to show my sincere gratitude to Prof. Masubuchi Yuichi for his support and encouragement on this thesis. I was interested in doing research on rheology, and I was so lucky to study with his support. I still remembered he pointed out the mistakes of my first paper patiently and encouraged me to think and continue.

I am also grateful to Assoc. Prof. Uneyama Takashi. Although his questions on my work were difficult to answer, I did make a progress by considering the tough questions. The most important thing I learned from him was to understand the research purpose clearly before going next.

Special thanks to Assit. Prof. Doi Yuya. I obtained many useful comments from him on my experiments, my papers, and group seminars. It was great to work with him.

I would like to thank Prof. Matsunaga Katsuyuki at Nagoya University and Prof. Sathish K. Sukumaran at Yamagata University for their suggestions on the thesis as deputy advisers. I would like to thank Prof. Watanabe Hiroshi at Kyoto University for his kind comments on my work at each conference. I would like to thank Prof. Ole Hassager at Technical University of Denmark and Prof. Nicolas J. Alvarez at Drexel University for their useful suggestions on the uniaxial elongational experiments. I would also like to thank Prof. Takano Atsushi at Nagoya University for his support on the fractionation experiments and GPC-MALS measurements.

I would like to thank Ms. Akagi Shizuka for her support on lab stuff. Many thanks to the lab members for the relaxed environment. We had a lot of interesting activities together. I really enjoyed life in the lab.

Finally, I wish to thank my parents for their love.

Nagoya, January 2022
Yang Lixin